Pergamon

Progress in Materials Science Vol. 38, pp. 425–474, 1994

0079-6425/94 $26.00

0079–6425(94)00006–9

FRACTURE SURFACES: A CRITICAL REVIEW OF FRACTAL STUDIES AND A NOVEL MORPHOLOGICAL ANALYSIS OF SCANNING TUNNELING MICROSCOPY MEASUREMENTS

Victor Y. Milman,*§ *Nadia A. Stelmashenko*† *and Raphael Blumenfeld*‡‖

*Solid State Division, Oak Ridge National Laboratory, Oak Ridge, TN 37831-6032, U.S.A.

†Cavendish Laboratory, University of Cambridge, Madingley Road, Cambridge CB3 OHE, U.K.

‡Princeton University, Princeton Materials Institute, Princeton, NJ 08540-5211, U.S.A.

CONTENTS

1. INTRODUCTION

The last decade has seen an important development that drastically changed the status of fractography as a branch of science. Instead of being purely descriptive collection of

§Present address: Molecular Simulations, The Quorum, Barnwell Road, Cambridge, CB5 8RE, U.K.
‖Present address: Center for Nonlinear Studies, Los Alamos National Laboratory, NM 87545, U.S.A.

observations, it is increasingly resorting to powerful mathematical apparatus and is effectively becoming a quantitative field. This achievement owes much to the introduction of the concept of fractal geometry for characterization of the morphology of irregular surfaces. To review the mathematical foundations of fractal geometry is outside the scope of this paper, and for a survey of this subject the reader is referred to Refs (1–3). However, only a few conceptually simple techniques are essentially needed in order to discuss the fractal features of the fractured surfaces. This was demonstrated in a seminal paper by Mandelbrot *et al.*[4] who introduced the main ideas and methods of the fractal analysis to the metallographic community. The wave of publications that immediately followed was dedicated to the application of essentially the same methods as in Ref. (4) to a variety of materials and types of fracture. As the amount of experimental data increased, it became possible to search for reliable correlations between the fractal properties of the fracture surface and the fracture toughness of material[4,5] and to study relative accuracy of different experimental techniques used in the fractal analysis.[6] In parallel, numerical simulations of the fracture process gained popularity and have become a very useful tool in the analysis. For example, these simulations can give estimates of fractal characteristics of the branching crack pattern for different models of material failure. Unfortunately, a recent review of this work by Herrmann[7] clearly shows that the predictions are essentially model dependent. It follows that reliable experimental data are significant both to distill the essential features that are required to generate a model for a given material, and to compare with the results of the simulations.

In this review we concentrate on the experimental techniques of the fractal analysis rather than discuss numerical modeling approach. There are several unresolved controversies, as well as important questions yet to be addressed despite the recent intensive activity in the field. First it is useful to have a compilation of the available experimental data. One of the difficulties in such a compilation is that there are strong variations in the fractal dimension measured in different studies, depending on the method of measurement. Therefore, part of the problem stems from the variety of experimental techniques combined with insufficient analysis of their comparative merits. Consequently, interesting data are sometimes misinterpreted as we show below. Another problem relates to the universality of the results, namely, the possible independence of the roughness exponent ζ on the specific material under study. This difficulty is amplified due to the fact that most of the fractal analysis results refer to a rather narrow interval of characteristic lengths that extend from 1 μm to 1 mm. Although measurements on such sizes can point toward existence of scale-invariance of the surface, it nevertheless fails to allow for accurate estimates of ζ. In fact many existing results for ζ are obtained from scaling over only one decade of, e.g. power spectrum of the height profile.[4] We suggest here that this difficulty is inherent to the fracture problem, and is independent of the quality of the measurements. To assist with this issue we propose a new analysis technique that goes beyond the conventional routine. The difficulty with the conventional approach is that in all methods only two-point correlations are analyzed to find the fractal dimension or the roughness exponent. This parameter is currently used as the only quantitative characteristic of the surface. Correspondingly, there appears to be no mathematical way to discriminate between two surfaces with similar fractal dimensions but different morphologies. Note that such discrimination is easily achieved by human eye and brain, which hints towards the missing link in the expansive attempts to find a relation between the fractal morphology of the surface and mechanical properties of the material.

We present here new results on fractures measured by scanning tunneling microscopy (STM) on surfaces in the nanometer scale. These results call into question contradictory universal relations found on micron scale.[8,9] The very existence of any such relationship is

of paramount importance. While it is traditional in materials science to search for global relations (perhaps in different analytic form for ductile and brittle fracture), the quest in this context is usually after correlations between measured quantities and mechanical properties. Although many experiments are carried out along these lines, the results are inconclusive. There are strong variations in the value of ζ, but in many cases there is no apparent correlation between its value and material properties. Nevertheless, there is a general agreement in the community of materials scientists that the higher the fracture toughness, the rougher the fracture surface, which *may* correspond to higher fractal dimension. However, at present this conjecture is yet to be substantiated. From the physicist's point of view, a universal fractal behaviour poses a challenge to explain such a fundamental law of nature. Since such a universal exponent should be independent of material characteristics then to material scientists such a result would mean that ζ is not a good quantity to monitor material properties. If, however, there are correlations between the roughness exponent (or roughness in general) and such properties, then this exponent is a useful tool in the attempts to improve materials strength or resistance to fracture.

One of our main aims here is to clarify this issue by compiling much of the experimental data and offering our view as to why this problem is so inherently difficult. Second, we suggest a novel method of characterization of the fracture surface, which employs information on the morphology of the structure beyond the two-point correlations. We believe that our morphology descriptor has an advantage in probing surfaces when searching for correlations with mechanical properties.

The outline of the present paper is as follows: We examine the fractal analysis techniques employed in fractography (Section 2). A critical review of the available experimental data is given in Section 3. We describe a new method of analyzing correlations in the surface structure,[10,11] which provides information additional to the fracture dimension (Section 4). Finally, we present in Section 5 an analysis of STM images of fracture surfaces of tungsten and graphite studied on the nanometer scale.

2. Techniques of Fractal Analysis of Surfaces

2.1. *Basic Definitions*

In analysis of surface topography one studies the height of the fractured surface, $h(\mathbf{r})$, as a function of the two lateral coordinates, $\mathbf{r} = (x, y)$. The two-point correlation function $C(\mathbf{r}) = \langle h(0)h(\mathbf{r})\rangle$(where $\langle \ldots \rangle$ stands for a surface average) is usually claimed to be represented by a power law for various kinds of surfaces. Let us first distinguish between a self-similar and a self-affine fractal. The former is invariant (statistically for real materials, or exactly for exact models) under *isotropic* dilation, namely when $x, y, h \rightarrow \lambda x, \lambda y, \lambda h$, while the latter is invariant under *anisotropic* dilation, namely, if $x, y \rightarrow \lambda x, \lambda y$, then $h \rightarrow \lambda^H h$.[1] H is the scaling exponent which is always in the range from 0 to 1 (sometimes referred to as the fractal codimension). Since most real surfaces scale differently in the plane of fracture and in the vertical direction, they are self-affine rather than self-similar. At large distances the self-affine fractal would look smooth and its global fractal dimension, D_g, would coincide with the Euclidean dimension (e.g. for surfaces $D_g \rightarrow 2$). Thus for a self-affine fractal the fractal dimension D can be defined only locally.[2]

There are several ways to define the fractal dimension of self-affine fractals. Let us consider, for the moment, the method of vertical sectioning of a rough fractal surface instead of

analyzing the surface itself. Such a section has a fractal (self-affine) profile, $h(x)$, with the fractal dimension $\mathbf{D}'$, which is related to the fractal dimension of the surface by:[1]

$$\mathbf{D}' = D - 1. \tag{1}$$

There are different definitions of $\mathbf{D}'$ (see eqs (2) and (3) below). These should all result in the same numerical value for a self-similar curve, *but not for a self-affine one*. For example, if we cover the curve with boxes of width $b\Delta x$ and of height $b\Delta h$, the box dimension $\mathbf{D}'$ is then defined by the scaling relation

$$N(b; \Delta x; \Delta h) \propto b^{-\mathbf{D}'}, \tag{2}$$

where $N(b; \Delta x; \Delta h)$ is the number of boxes needed to cover the curve. For boxes that are small compared to the typical range of heights of the profile, it is possible to derive a significant relation between the fractal dimension and the scaling exponent:[2]

$$\mathbf{D}' = 2 - H. \tag{3}$$

For a one-dimensional profile we can evaluate yet another fractal dimension by applying a ruler of length δ to measure the length L along the curve. In this way we obtain the so-called divider dimension D_d,[2]

$$L \propto \delta^{1-D_d} \propto \delta^{1-1/H}. \tag{4}$$

Therefore the local divider dimension is $D_d = 1/H$ while the box dimension for the same profile would be $2H$. For a self-affine surface H is more suitable a characteristic than D because it does not depend on the method of analysis. In Section 2.2.2 it is shown that H coincides with the roughness exponent introduced in Ref. (8). Let us now briefly review the methods available to measure this exponent. One should bear in mind that these techniques usually assume self-affinity and then go on to exploit certain relational consequences of this property when analyzing experimental data. Since it is not at all clear that every fracture is self-affine, then results obtained from such analyses should always be checked to validate this assumption.

2.2. *Perpendicular Sectioning Method*

Technically this method consists of taking a vertical section through the fracture surface. Usually the cut surface is further polished and then studied in a scanning electron microscope or in an optical microscope. The micrographs are digitized and the height profile is extracted and analyzed. For reasons to be detailed later this technique is used for fractal surface analysis in spite of its obvious disadvantage of destroying the sample. There are alternative non-destructive methods that can be used instead of the physical sectioning to provide the same information. For example, the height profile can be recorded using precise profilometer.[8] Unfortunately, a profilometer does not allow to probe down to the micron length scale. Another method to measure surface height[12] is by a line scan of brightness in the scanning electron microscope (SEM). Whether such a scan indeed represents the height profile function is yet to be established convincingly, but experimental evidence suggests that this is true.

Having obtained the function $h(x)$ by any of those methods, it is then analyzed using one or more techniques described below to determine the value of either $\mathbf{D}'$, D_d or H. The reader should note that in principle, there is no reason for $h(x)$ to be single-valued, especially in cases of extensive crack branching observed in some materials. In fact, a multi-valued $h(x)$ can be found by vertical sectioning.[13] It should be noted though that only actual cutting can reveal such structure, while profilometer[8] or electron microscope[12] would always produce a

single-valued function. Clearly, care should be exercised when applying methods based on, e.g. Fourier analysis to multi-valued profile functions.

2.2.1. *Profile length measurement*

In most cases the digitizing software provides the means to evaluate the length of the curve using rulers of different sizes, δ. From eq. (4) we have for the scaling exponent:

$$D_d = 1 - \frac{d \log L}{d \log \delta}, \tag{5a}$$

$$H = 1/D_d. \tag{5b}$$

The shortest ruler length used in such experimental measurements so far is of the order of 1 μm. Usually the $\log L$–$\log \delta$ plot (the Richardson plot) is only approximately linear.[14] A breakdown of linearity should occur at high values of δ where the system becomes homogeneous. When this happens, the Richardson plot saturates to a horizontal plateau. To complicate the issue the length of the profile approaches a finite limit at small δ as well,[15,16] where a microscopic structure of the profile starts to be probed. An increase of magnification beyond this scale cannot be related to the self-affinity in the meso-scale. The conjecture[14] that the limit of $L(\delta)$ for $\delta \to 0$ gives a 'real' length of the curve instead of the infinity that is expected for the 'ideal' fractal curve could be considered seriously only if applied to the profiles recorded on the atomic scale, and not on the scale of microns.

2.2.2. *Pair correlation function and Fourier analysis*

Let us now define some functions that are used in this method. The height autocorrelation function, $C(x)$, is:

$$C(x) = \lim_{L \to \infty} \frac{1}{L} \int_0^L (h(x' + x) - \langle h \rangle)(h(x') - \langle h \rangle)\, dx'$$

$$= \lim_{L \to \infty} \frac{1}{L} \int_0^L h(x' + x) h(x')\, dx' - \langle h \rangle^2 \tag{6}$$

where the average height, $\langle h \rangle$, of the profile is given as:

$$\langle h \rangle = \lim_{L \to \infty} \frac{1}{L} \int_0^L h(x)\, dx. \tag{7}$$

The pair correlation function, $G(x)$, is defined as:

$$G(x) = \lim_{L \to \infty} \frac{1}{L} \int_0^L [h(x' + x) - h(x')]^2\, dx'. \tag{8}$$

Opening brackets in this equation and substituting $C(x)$ from eq. (6), leads to a simplified relation between the pair correlation function and the autocorrelation function:

$$G(x) = 2(\omega^2 - C(x)) \tag{9}$$

where we define the width of the profile, ω, as

$$\omega^2 = C(0) = \langle (h - \langle h \rangle)^2 \rangle. \tag{10}$$

The fractal dimension can be extracted from the analysis of the behaviour of $G(x)$ at small x.[3] If in this regime $G(x)$ follows a power law,

$$G(x) \propto x^{4 - 2D'}, \tag{11}$$

then we expect the box dimension to be equal to $\mathbf{D}'$.[2] Thus we have the following expressions for the fractal dimension and for the scaling exponent:

$$\mathbf{D}' = 2 - \frac{1}{2}\frac{d\log G(x)}{d\log x} = 2 - \frac{1}{2}\frac{d\log[C(0) - C(x)]}{d\log x}, \tag{12a}$$

$$H = 2 - \mathbf{D}'. \tag{12b}$$

Equation (11) holds only on scales smaller than the correlation length in the direction parallel to the surface. At longer distances the log–log plot saturates as shown below.

Though the autocorrelation function can itself be measured and analyzed in order to derive the value of H according to eq. (12b), it is common to use its Fourier transform, $h(f)$, or the power spectrum, $p(f)$, of the profile:

$$h(f) = \int h(x)\exp(ixf)\,dx, \tag{13a}$$

$$p(f) = |h(f)|^2 = \int C(x)\exp(ixf)\,dx. \tag{13b}$$

From the scaling behaviour of the autocorrelation function for small x it is then possible to derive the asymptotic behaviour of the power spectrum at infinity:

$$p(f) \propto f^{2\mathbf{D}'-5}, \tag{14a}$$

which can be recast in the form:

$$\mathbf{D}' = \frac{5}{2} + \frac{1}{2}\frac{d\log p(f)}{d\log f}. \tag{14b}$$

The value of H is then given by eq. (12b).

The power spectrum determined experimentally is usually strongly affected by statistical fluctuations that introduce significant error in the value of the fractal dimension. To reduce these fluctuations it was proposed to analyze the integrated power spectrum,[4] $P(f)$, defined as

$$P(f) = \int_f^\infty p(f')df'. \tag{15}$$

For frequencies higher than the inverse of the correlation length the power law behaviour gives:

$$\mathbf{D}' = 2 + \frac{1}{2}\frac{d\log P(f)}{d\log f}. \tag{16}$$

A simple formula relates the scaling properties of the power spectrum with the scaling of roughness, ω. To derive this relation we take the inverse Fourier transform of eq. (13b) and evaluate $C(x = 0)$:

$$\omega^2 = C(0) = \int_{f_{\min}}^\infty p(f)df \propto f_{\min}^{2\mathbf{D}'-4}. \tag{17}$$

The length of measurement is finite L_0, supplying a lower limit $f_{\min} = 2\pi/L_0$ to the integral, which plays an essential role here.[2] Substituting this lowest spatial frequency into eq. (17) we obtain for the roughness scaling:

$$\omega \propto L_0^{2-\mathbf{D}'} \propto L_0^H. \tag{18}$$

2.2.3. *The return probability histogram*

Yet another method of analysis of the height profile has been suggested recently by Måløy *et al.*[8] They evaluate the return probability histogram, $R(\Delta)$, which is the probability for a height y appearing at a given position x to reappear for the first time at a position $x + \Delta$, averaged over all x. This probability is related to the chord length distribution and it scales as:

$$R(\Delta) \propto \Delta^{H-2} \propto \Delta^{-D'}, \tag{19a}$$

$$\mathbf{D}' = -\frac{d \log R(\Delta)}{d \log \Delta}. \tag{19b}$$

The return probability histogram may be easier to calculate, for a given profile $h(x)$, than the Fourier transform, but the method seems to have some drawbacks. We will discuss this issue when describing our experimental results in Section 5.

2.2.4. *The variation method*

This technique has been recently suggested by Dubuc *et al.*[17] They demonstrated that this method was more accurate than any other technique of the fractal analysis of self-affine curves, at least when applied to few analytically constructed profiles with a predetermined fractal dimension. This test has been carried out in Ref. (17) for $\mathbf{D}'$ in the range 1.4 to 1.6, which is higher than the values observed for fracture surfaces. Further testing[18] has shown that the variation method estimates accurately the fractal dimension of the Weierstrass–Mandelbrot function when $\mathbf{D}'$ is in the interval 1 to 1.6.

The method relies on the following properties of a fractal function $h(x)$: it should be continuous and almost nowhere differentiable. As an illustration of the underlying idea let us consider a straight line connecting two points on the curve, $(x, h(x))$ and $(x', h(x'))$. The upper limit of the absolute value of the slope of this line is infinite when x' tends towards x, and the rate of this infinite growth is determined by the fractal dimension of the curve. The analysis is carried out as follows: Let us introduce a ϵ-oscillation, $v(x, \epsilon)$, according to the following definition:

$$v(x, \epsilon) = \max h(x') - \min h(x'), \quad |x' - x| < \epsilon, \tag{20}$$

and define the integral (termed the ϵ-variation) $V(\epsilon)$:

$$V(\epsilon) = \int_{L_0} v(x, \epsilon)\, dx. \tag{21}$$

The limit of $V(\epsilon)$ for $\epsilon \to 0$ is zero due to the continuity of the function $h(x)$. But the rate at which $V(\epsilon)$ scales when $\epsilon \to 0$ is:[17]

$$V(\epsilon) \propto \epsilon^{2-\mathbf{D}'}, \tag{22}$$

which provides another way to calculate $\mathbf{D}'$. The fractal variation analysis can be interpreted as a numerical technique of box counting.[18] Detailed description of the method including computational algorithm can be found in Ref. (17).

2.3. *Slit Island Method (SIM)*

With this technique, suggested by Mandelbrot *et al.*,[4] one analyzes horizontal sections of the fracture surface. The surface to be probed is covered with a thin layer of a material with

different optical reflectivity. A subsequent polishing reveals islands of the main material that grow and merge as polishing progresses deeper. Applying this procedure to isotropic surfaces produces *self-similar* patterns since all in-plane directions are equivalent. Therefore this approach has the advantage of having an unambiguous definition of the fractal dimension. Its value is $\mathbf{D}' = D - 1$ since the pattern is created by sectioning a surface with dimension $D > 2$ with a two-dimensional plane.[2] The fractal dimension D is derived from the scaling behaviour of the 'coastlines', D_{coast}, via $D = D_{\text{coast}} + 1$. This relation reflects the simple fact that the fractal surface is sectioned by a Euclidean plane. Comparing with eq. (1), this relation also indicates that $D_{\text{coast}} = \mathbf{D}'$.

The set of coastlines obtained in these parallel sections can be analyzed in two ways. First, the divider dimension can be found from the measurement of the perimeter, $\mathscr{P}$, with different rulers, δ:

$$\mathscr{P} \propto \delta^{1-\mathbf{D}_d}, \tag{23a}$$

$$\mathbf{D}_d = 1 - \frac{\mathrm{d}\log \mathscr{P}}{\mathrm{d}\log \delta}. \tag{23b}$$

The use of eq. (23a) seems somewhat superior to eq. (5a) although they look similar. The difference is that now the self-similar curve is analyzed and not the self-affine one. Note that the scaling exponent, H, is now given by eq. (12b) rather than by eq. (5b).

Another way of using SIM is to apply the perimeter-area scaling relationship to coastlines.[4] When the area, $\mathscr{A}$, and the perimeter, $\mathscr{P}$, are measured for a set of 'islands' using the same ruler length, we have for the *self-similar* curve:

$$\mathscr{A} \propto \mathscr{P}^{2/\mathbf{D}'}, \tag{24a}$$

$$\mathbf{D}' = 2\frac{\mathrm{d}\log \mathscr{P}}{\mathrm{d}\log \mathscr{A}}. \tag{24b}$$

A wrong form of the perimeter–area relationship, $\mathscr{A} \propto \mathscr{P}^{\mathbf{D}'}$, can be found quite often in the literature, e.g. Refs (19) to (22). This was probably inspired by a misprint in Ref. (4) where Mandelbrot *et al.* used the correct relations (24a,b) for their fractal analysis, but erroneously quoted $\mathbf{D}'$, rather than $\mathbf{D}'/2$, for the slope of the curve of $\log \mathscr{P}$ vs. $\log \mathscr{A}$. As a consequence of this conclusion, Ray *et al.*[20] found that D *increases* with toughness. We have re-analyzed their data with the proper form of eq. (24) and found that D *decreases* with toughness.

There exists some controversy related to the use of the perimeter–area relation for the fractal analysis of real surfaces. The problem is in the dependence of both $\mathscr{P}$ and $\mathscr{A}$ on the ruler length, δ. In principle, eq. (24) holds only in the limit of small δ. At intermediate values of δ the measured perimeter becomes affected by the regular part of the coastline present in the image.[2,5,6] It is not clear whether the dependence of D on δ in this method has a physical origin, or whether it is an artifact of the measurement technique. This raises doubts regarding the validity of the limiting value of D observed at very small δ. In most cases, however, the results obtained with small enough rulers agree with the data obtained by other methods. The most controversial result, using small rulers, shows that D increases with the fracture toughness, while the opposite tendency emerges from using bigger rulers.[5,23] We will comment on these findings in Section 3.

There is an advantage in using eq. (24) when compared to the perimeter–ruler length

relation, eq. (23). In the latter case the value of $D_d - 1$ is measured which has a high relative error for $D_d \approx 1$. This means that the curve of $\log \mathscr{P}$ vs. $\log \delta$ has a very moderate slope and any noise or non-linearity would make accurate measurements difficult. The plot of $\log \mathscr{P}$–$\log \mathscr{A}$ behaves much better and usually has an easily identifiable linear part.

A recent development in SIM involves a particular form of computer analysis, which allows for using this method non-destructively. For example, Nogués *et al.*[24] used three-dimensional STM images to perform such an analysis. It is convenient to think of this method as of filling an imaginary three-dimensional relief with water up to different levels and then examining the coastline of the obtained islands. This method suffers at present from the too coarse grid used by commercial STM (e.g. 256 × 256 pixels), which means that the ruler length cannot be reduced to sufficiently small sizes. This is a serious limitation as long as the question of the importance of the ruler length in the perimeter–area analysis is still unresolved. However, as high resolution imaging with long scans becomes attainable, the advantage of being non-destructive would probably tip the scales in favour of this technique.

The coastlines analyzed by SIM can be considered as either islands within lakes, or as lakes within islands. In the context of fracture there are always two corresponding surfaces, which are both available, in principle, for scrutiny. It is noteworthy that in purely brittle fracture the islands on a sectioned image of one surface should match exactly the lakes on the corresponding section of the other surface. In ductile material with void coalescence, on the other hand, the lakes on one surface match the *lakes* on the corresponding surface, as has been found in fractured steel.[25,26] The latter phenomenon can also be observed when fracture is accompanied by relaxational processes. Thus it is important to determine in what class of processes does the fracture fall before analyzing and comparing the two surfaces. Usually, being in different classes also results in different toughness characterizations. Moreover, the standard 'islands within lakes' interpretation[4] can give values of D that are different from those obtained when the 'lakes within islands' approach is assumed. This indeed seems to be the case for the fractured ductile steel studied in Ref. (25). There the difference in the roughness exponent, calculated using these two interpretations, was shown to increase as a function of material toughness and indeed to vanish for brittle fracture. In that particular study, the two ways of analysis even give an opposite dependence of D on the toughness. This demonstrates that it is important to adopt the standard 'islands within lakes' choice for analyzing the surface.

A final comment is in order regarding the background subtraction, which is usually done before carrying out any kind of numerical analysis. This step would not be necessary if an infinitely small ruler could be used. But with a finite ruler length and with a macroscopic tilt of the image one effectively introduces a regular component that can affect measured fractal properties. In our opinion, the least ambiguous technique is to subtract the least square fitted plane (a straight line for a profile) from the image. We show in the Appendix that this minimizes the roughness defined by eq. (10), and so allows to treat only the inherent fractal structure of the profile. In quite a few studies the linear background is taken as the line connecting the first and the last point of the profile (e.g. Ref. (8)). Although it need not change the results significantly, this nevertheless seems to be a rather arbitrary choice. This arbitrariness can be altogether obviated by using the cosine Fourier transform for the spectrum instead of the complex Fourier transform. For methods not based on spectral analysis there is no good reason for such a choice of the background. It should be mentioned though that there is a disadvantage in tilting the entire plane because particular cuts through the surface may still retain a nonzero average slope after the tilt.

2.4. *Direct Surface Area Measurement*

An alternative technique for fractal analysis of surfaces has been developed very recently and applied to two different experimental methods.[27,28] The underlying idea is to generalize the divider method to two-dimensional objects. Instead of studying scaling behaviour of the profiles obtained in the surface section, Denley[27] and Friel and Pande[28] analyzed directly the dependence of the area of the fractured surface on the length scale. The following scaling relationship should hold for a self-affine surface in the limit of $\delta \rightarrow 0$:

$$S = S_0 \delta^{2-D}. \tag{25}$$

This relation resembles eq. (5a), but δ is now the length of the side of the elementary square used for coverage in the area measurement. The roughness exponent is given as $H = 1/(D-1)$ because D in eq. (25) is the divider dimension.[2] Equation (25) has been considered by many authors as an appealing alternative to traditional methods based on the profile analysis, but so far has not found a wide application due to the experimental difficulties in measuring the area.[12,15]

In Ref. (27) this measurement was carried out by integrating the area of the surface of the STM image that was recorded on the square grid of pixels. This procedure was repeated for the data considered at points with varying spacings thus producing the S (δ) plot. More recently Friel and Pande combined this method of analysis with the stereoscopic SEM imaging.[28] The basic idea is to compare SEM images recorded at two different tilt angles of the electron beam. The main computational problem is to identify corresponding points in a pair of stereo images, and this can be overcome by using modern image analysis software.

These two methods, STM and stereographic SEM, seem to be unique in that they can provide with sufficient accuracy a true morphology. Moreover, they complement each other with respect to the length scale. STM usually has 10 μm as the highest scan range available, while SEM starts imaging from approximately 1 μm going up to 100 μm. We will discuss later serious limitations imposed by the current state of the development of these microscopies. However, we believe that the future of the analysis of surfaces belongs to such non-destructive methods capable of capturing a three-dimensional surface image. Implementation of these techniques should not be confined to area scaling analysis, because any other method can be applied once the surface image is obtained. In particular, we will illustrate in Section 5 an application of the higher-order correlations analysis performed using STM images.

2.5. *Determination of Scaling from Measurement of Non-Structural Properties*

Another approach to the fractal analysis consists of studying the dependence of certain non-structural properties on the surface geometry. For example, scattering experiments measure the structure factor, $S(q)$, which is related to the Fourier transform of the height correlation function. Consequently, power law scaling can be expected for $S(q)$ for fractal objects, as has been indeed observed in studies of colloidal aggregates.[29]

The roughness of the surface influences chemical and electrochemical processes that take place in the near-surface layer. It can be shown that there is an exact mapping in the mathematical formulation between the DC electrical response of an electrode, the diffusive response of a membrane, and the steady state yield of a heterogeneous catalyst.[30] Using this mapping the fractal nature of fracture surfaces has been recently probed electrochemically by studying the dependence of the Faradaic current in the diffusion limited process on the surface area.[31] For this experiment an electrochemically inert electrode is immersed into an

electrolyte containing some inert salt of high concentration and an electroactive substance of low concentration. A golden replica of the fracture surface is then used as the electrode.

For a simple planar case the direct current in this experiment is proportional to $t^{-1/2}$, where t is time, and to the diffusion front area, A. This particular time dependence follows from the fact that the charge passing through the interface corresponds to the number of electroactive species in the diffusion layer of thickness $\Delta \propto (\mathscr{D}t)^{1/2}$, where $\mathscr{D}$ is the diffusion coefficient in the medium with the rough boundary. With time, this layer becomes thicker and the surface area changes. The diffusion layer width can be regarded as a time-dependent length of the ruler that is used to measure the area of the fractal surface. The Cottrell equation[31] for the current,

$$I \propto A(t)\sqrt{\frac{\mathscr{D}}{t}} \propto \frac{A(t)\Lambda}{t}, \tag{26}$$

can be reformulated in terms of the volume, $V(\Lambda)$, located within a distance Λ from the fractal surface:[30]

$$I \propto \frac{V(\Lambda)}{t} \propto \frac{\Lambda^{3-D}}{t} \propto t^{(1-D)/2}. \tag{27}$$

Here we have used the above mentioned dependence, $\Lambda \propto t^{1/2}$, and the fractal scaling of the volume as determined by the exterior Minkowski–Bougiland dimension, D. This dimension is defined through the volume, $V\epsilon$, which lies within a small distance ϵ of the electrode,

$$D = \lim\left(3 - \frac{\ln V\epsilon}{\ln \epsilon}\right), \quad \epsilon \to 0. \tag{28}$$

The same experimental arrangement can be used for AC measurements of the frequency dependency of the admittance, Y. From arguments similar to those given above but with $\Lambda \propto (\mathscr{D}/\omega)^{1/2}$, we have:[30]

$$Y \propto \omega^{\frac{D-1}{2}}. \tag{29}$$

The method has certain experimental limitations which become obvious when one compares the ideal situation described above with real measurements. The most important requirement is to have zero solution resistance which ensures that the volume of electrolyte is equipotential. Otherwise the response of the electrolyte to the potential drop at the surface cannot be easily related to the local (fractal) properties of the interface. Another problem is that since the replica method cannot reproduce the fine structure of the original surface, it is likely to reduce the regime over which the scaling can be measured. To test this issue we suggest that an analysis of both matrix and replica be carried out with conventional imaging to establish their equivalence.

3. Experimental Data on Fractal Characteristics of Fracture Surfaces

3.1. *Why is the Fracture Surface Fractal? How Universal is this Feature?*

The concept of fractals when applied to fracture is useful not merely as another method for describing the surface morphology but as a possible lead to a better understanding of the underlying differences between fractures. In particular two questions seem pertinent. Why is the fracture surface expected to be fractal? What is the relation between fracture surface characteristics and material properties?

There seem to be good reasons for the surface to have fractal scaling, although these reasons may differ for different kinds of fracture. For slow brittle fracture (brittle intergranular, transgranular cleavage) a simple calculation of the stress field shows that the moving-boundary problem has scale invariant solutions that couple very strongly to the inherent instability of the cracking process and produce self-similar patterns.[32] The situation is equivalent to many scalar free-boundary problems such as dendritic solidification, viscous fingering, diffusion limited aggregation, electrodeposition, etc. In the case of a slowly propagating crack the resulting pattern is more complex than in those scalar growth problems due to the tensorial nature of the stress field. Nevertheless, there is a strong qualitative similarity between the different processes. For a dynamical crack propagation (namely, when the propagation rate is a substantial fraction of the Rayleigh wave speed), the process very much resembles breakdown processes in dielectric media, which is known to produce fractal trajectories. The similarity in the formulation of the problem thus suggests that we may expect fractal features in the resulting fracture surfaces too.

From another point of view, the growth of the brittle crack can be considered as a process of the energy transfer from the macroscopic level to the microscopic one with its final release at the crack tip. In this case the fractal dimension of the fracture structure is shown to be related to the radial scaling of the stress at the crack tip and to the intensity of the energy dissipation.[33]

In ductile materials the fracture propagates as a result of the formation, growth and coalescence of microvoids near the crack tip. This process is not understood currently well enough. Nevertheless, some analogies have been drawn between this process and the percolation problem[1,34], which also leads to a fractal pattern.

Ductile fracture of metals is always preceded by a certain amount of plastic deformation. There are currently both experimental[34–36] and theoretical[37] evidences in favour of the fractal character of the plastic slip. The slip line patterns on the surface of deformed sample reflect cooperative motion of interacting dislocations that might involve self-organization to some degree. The fractal analysis can be easily applied to a system of parallel slip lines. A straight line drawn perpendicular to the lines generates a set of points that can be studied using either box counting method, the yardstick method, or the gap distribution analysis.[35] The fractal dimension of such sets has been found to be 0.45 ± 0.10 for coarse slip of a copper single crystal;[35] 0.30 ± 0.15 for fine slip of a cobalt single crystal;[35] 0.49 ± 0.03 for a fine slip of a cadmium single crystal.[35] All these results refer to the length scale from 60 to 2000 nm. The discontinuity of plastic deformation can be observed in the stress–strain curve recorded at very low temperature. It has been shown that, for example, austenitic steels tested at 4 K exhibit serrated stress–strain characteristics and a discontinuous pattern of temperature growth.[37] The distribution of the temperature growth reflects the spatial distribution of the slip process, and analysis finds a fractal dimension of 0.7 for this structure. This value is close to that of the dyadic Cantor set (0.63), which is why it has been speculated that work hardening leads to redistribution of microscopic necking under tension in a way that is similar to the procedure involved in the construction of the Cantor set.[37] Phenomenological modeling using a cellular-automaton approach suggests that work hardening should result in a low fractal dimension of the set of slip lines equal to 0.25 ± 0.10. Work softening, on the other hand, should produce higher values of order 0.45 ± 0.10.[38]

Thus it seems that in either fracture mode, dynamical process of material failure leads to patterns with statistics that depend on the very general parameters, such as the dimension of space, rather than on the microstructure. This may imply that the structure of fracture surfaces is universal, and in fact it has been conjectured recently that there is a universal value

of H, around 0.80 for ductile fracture[9] and 0.87 for brittle fracture.[8] This, however, contradicts any idea of correlation between H and the fracture toughness because a 'universal' value denies any dependence of the fracture characteristics on specific material properties. Statistical analyses of a large body of existing data for a variety of materials is given below which indicates that the value of H actually lies in a wide interval from 0.6 to 1.0. This scatter *in the exponent* is far too high for any universality hypothesis to account for. Måløy *et al.*[8] supported their conjecture on the universal value of H by comparing several measurements with the results from a computer experiment[39] that produced $H = 0.7$ for a two-dimensional model with a few different types of bonding disorder. There are several problems with such a bold conjecture: (i) It is difficult to apply results of two-dimensional simulations to the three-dimensional experiment data; (ii) There exist many other models that simulate fracture, each capturing certain essential features of the real process, and it appears that the results of these simulations are strongly model-dependent. Indeed, results for simulated fractures result in a value of H that spans the entire range from 0.3 to 1.0.[7] Thus, at present, it is difficult to see how the computer modeling results can be used to support the universality hypothesis.

It has been suggested by different authors that fracture may proceed along so-called minimal surface.[40,41] Such a surface corresponds to a global minimum of the fracture energy that is achieved by optimizing the direction of the crack growth at each time step. When applied to porous or composite materials such a surface simply minimizes the intersection area with the matrix.[40] The minimal surface was shown to be self-affine with a roughness exponent estimated as 0.50 ± 0.08.[41] This value is significantly lower than the suggested universal exponent.[8,9,13] However, this value of H may suggest that in this model the crack should follow a Brownian path which is known to yield $H = 1/2$ exactly. Bouchard *et al.*[13] have suggested recently that the minimal surface cannot be reached dynamically, at least on a macroscopic or mesoscopic structural level. If so then the fracture surface available for examination is determined by kinetic processes rather than by equilibrium energetics of fracture.

In the following two subsections we give a review of existing data on fractal properties of brittle and ductile fracture surfaces.

3.2. *Brittle Fracture*

Most of the results given in this subsection refer to ceramic materials, while the rest of the data concerns brittle and quasibrittle fracture of metals (low temperature or stress corrosion cracks). It is well established that the surface around the fracture-initiating brittle crack can be divided into regions with qualitatively different morphology.[42–44] The first relatively smooth growth region (mirror) is followed by increasingly coarser zones (mist and hackle). This pattern ends with a macroscopic crack branching region.[42] The traditional metallographic data tended to analyze the entire surface, lumping together information from all regions, and therefore inevitably obscuring any distinction between them. Reports of separate analyses on different zones are very rare.[43,44]

3.2.1. *Ceramics and glasses*

Tsai and Mecholsky[43] studied the fracture surface of single-crystal silicon using the SIM technique and eq. (23) for the perimeter–ruler scaling. A controlled flaw (hardness indent) was introduced on either (100) or (110) surface of the sample that was subsequently fractured in bending so that the flaw was on the tensile side. The accuracy of the fractal analysis should

be quite low as the ruler lengths used in that study ranged in a very short interval, from 10 to 120 μm. Separate data are reported for the mirror region (smooth), crack branching region (rough) and post-branching region (again smooth). They found that H was 0.90 ± 0.04 in the branching region on (100) surface and 0.96 ± 0.04 on (110) surface. The roughness exponent for both mirror and post-branching region was 0.99 ± 0.01, thus confirming existence of a non-fractal Euclidean geometry.

Langford *et al.*[44] used STM images with scan sizes that ranged from 25 to 260 nm to analyze the fracture surface of MgO. The minimum length step was approximately 0.4 nm. They used both power spectrum analysis with eq. (14) and box counting using eq. (2). The latter method should be more reliable in their measurement because the one-dimensional Fourier analysis was carried out only on 256 point grid, introducing a very large error. The least squares fitted plane has been subtracted before the fractal analysis was carried out in order to correct for macroscopic tilt. The sample was fractured in the three-point bending test and separate sets of data were given for the structure of tensile and compressive sides of the specimen. Both methods of analysis gave a value of $H = 0.6 \pm 0.1$ for the tensile side. It was impossible to distinguish within the experimental error between the values of H for the smooth mirror region and for the crack branching zone. On the compressive side few regions were found with the same scaling as on the tensile side. However, a number of images taken on the compressive side have shown a non-fractal behaviour.

Mecholsky *et al.*[45] studied surfaces of six kinds of alumina and of five glass-ceramics (zinc silicates and lithia borosilicate) by employing a variety of techniques. They applied SIM with the ruler length from 0.4 to 100 μm by using eq. (24) for the perimeter–area scaling, and also by Fourier analysis using eq. (16) for the integrated power spectrum scaling. All methods gave consistent values of $H = 0.77 \pm 0.08$ for alumina and 0.88 ± 0.06 for glass-ceramics. They found no systematic dependence of D on the ruler length in SIM analysis contrary to the data of Lung and coworkers for steels.[5,23] They fitted the relation between D and the critical stress intensity factor, K_{IC}, with the form:

$$K_{IC} = K_0 + E a_0^{1/2} (\mathbf{D}' - 1)^{1/2}, \tag{30}$$

where K_0 is the value of K_{IC} for the hypothetical material with the smooth fracture surface, E is Young modulus, and a_0 is a parameter that has units of length. It has been argued[45,46] that this parameter can be interpreted as the characteristic dimension of the fracture zone around a crack tip.

Relation (30) was used by Mecholsky and Freiman[42] to discuss a connection between the value of D and the radii, r_j, of the different regions of the fracture surface as defined above. They have conjectured a relation of the form $r_j \propto 1/(D-2)$, although this is to be taken cautiously in view of the poor data statistics. The values of H in Ref. (42) are 0.91 for borosilicate glass and for calcium aluminosilicate glass; 0.88 for (100) surface of silicon; 0.83 for pyroceram 9606 and for ZnS; 0.80 for partially stabilized zirconia; 0.78 for cobalt-bonded WC composites; 0.67 for alumina and for ZnSe. All these results were obtained by SIM using eq. (23) for the perimeter–ruler scaling. Details of the measurement procedure for borosilicate and calcium aluminosilicate glasses are given in Ref. (46). Polishing these glasses resulted in their fragmentation, and therefore a double replication technique was used. Scanning electron microscopy confirmed that structural features bigger than 5 μm were preserved during the preparation of the positive replica. This study is questionable not due to the replication procedure, but rather because the authors used too small a range of ruler lengths, from 6 to 40 μm. It is very difficult to support existence of scaling by studying less than one decade in length scales. Therefore the authors' conclusions[42,46] regarding existence of a connection

between the radii in the mirror zone and the fractal dimension cannot be substantiated by their results and requires further investigation.

A rather puzzling result was reported by Mitchell and Bonnell from the STM investigation of silicon single crystal fractured on the (111) cleavage plane.[47] Statistically reliable profiles were acquired with a step of approximately 0.3 nm and a total scan length of 1000 steps. The value of H was estimated from the integrated spectrum $P(f)$, eq. (16), to be equal to 0.93 ± 0.07. However, when we have tried to calculate H using the plot given in that paper for $p(f)$ by using eq. (14) we find that $H = 0.31$. This discrepancy, which cannot be reconciled by any error bars, is not addressed by the authors, and it is possible that there exists some error in their numerical procedure. This is most unfortunate because this case is one of the very few studies in the nanometer scale, which is so far the least studied length scale.

Mecholsky and Mackin applied the SIM using both eqs (23) and (24) to study fracture surfaces of a naturally occurring silicate (flint).[48] Relation (30) was corroborated, indicating that rougher surfaces correspond to higher material's resistance to fracture. The value of H has been found to be 0.85 for brittle transgranular fracture, 0.75 for mixed transgranular and intergranular fracture and 0.68 for intergranular rupture.

Baran *et al.*[49] carried out mechanical profilometry of the fracture surface of three dental porcelains and of experimental glass P2V25. A 2 mm length of the profile was surveyed with 2 μm ruler length. The variation method was used to calculate fractal dimension, see Section 2.2.4. No mirror or mist regions were found on the surface of any material, probably due to the presence of precipitate particles in all cases. The roughness exponent was 0.93 ± 0.04 for the glass fracture surface, and it varied from 0.67 to 0.84 for porcelains. Their results indicate that K_{IC} decreases slightly when D increases, opposite to other reports concerning brittle materials. However, this effect is too small compared to experimental errors and hence may not be indicative. Scaling of the ϵ-variation as described by eq. (22) was observed over not more than one decade in case of porcelains, and thus the error in D should be not less than 0.1, which casts some doubts on whether the fractal description is useful at all for this analysis.

Miller and Reifenberger[18] applied the variation method to analyze STM images of a fractured carbon surface. The surface was prepared by shattering a rod made of a medium-grain carbon. One-dimensional scans consisting of 2048 points were recorded with the total scan lengths that varied from 0.5 to 5 μm. Individual scans exhibited nicely linear plots corresponding to eq. (22) in logarithmic coordinates with scaling showing over nearly two decades. However, there is a substantial scatter in the measured values of the roughness exponent depending on the scan direction and its length. Low-resolution images with 1–5 μm scan size produced H from 0.44 to 0.50 which is substantially lower than results reported in the micron range using other methods. Two-dimensional version of the variation method has been applied to 128×128 images to yield $H = 0.43$ in agreement with data from one-dimensional profile analysis. The roughness exponent for scans shorter than 1 μm was found to be substantially higher, from 0.65 to 0.84, and to increase systematically as the scan size decreases. This increase of H may be attributed to the fact that STM approaches the atomic resolution, cutting off the fractal behaviour. Alternatively, the effect may be explained by the influence of noise which becomes more important on a shorter length scale as we have found in our study (Section 5). A third possibility for the origin of this effect may be that at higher magnification results are distorted by the convolution of the true profile with the shape of the STM tip.

Lin and Lai[50] measured the fractal dimension of fractured surfaces in a series of carbon fibre-reinforced composites with different fibre contents. They used SIM and found scaling within the area–perimeter relation in the range from 5 to 100 μm. The fracture process was

cleavage of polyether sulphon (PES-C) matrix accompanied by localized plastic deformation near the fibre–matrix interface. The roughness exponent can be derived from these results to range from 0.62 to 0.90. In this study a systematic decrease in the fracture toughness is observed with increasing fractal dimension. However, this dependence is found to be weak and amounts to 26% drop in K_{IC} when $\mathbf{D}'$ increases by 0.3.

Fractal character of crack propagation in epoxy and epoxy composites has been studied in detail by Ma Zhenyi *et al.*[51] Notched samples of Epon 828-Z epoxy with different concentrations of alumina filler were fractured in tensile loading in a vacuum chamber. The photon emission signals were recorded during fracture, and optical and electron microscopy were used in a subsequent study of the fracture surface. The photon emission intensity as a function of time was found to be characteristic of deterministic chaos rather than Markovian. Observations on the microscopic level support the idea that fracture in all cases was due to crack propagation in the epoxy matrix and has no interfacial component which may correspond to fracture of alumina particles. Assuming that the photon emission signal is caused by bond breaking and possibly by the recombination of defects created by this process, these results suggest that the crack growth can be characterized by dynamics that lead to a fractal structure. Further examination of the surfaces using SIM and the area–perimeter scaling produced linear plots in logarithmic coordinates with the roughness exponent of 0.75 ± 0.05. In our opinion the system studied in this work may be useful for testing predictions of the theoretical models upon.[7] This is so because in this case there exists information on both the dynamics of the crack growth and on the fractal structure of the resulting surface. Moreover, the fracture process is described by bond breaking, while atomistic fracture of metals requires more sophisticated modeling.

Måløy *et al.* reported values of H for several different materials: 0.90 for graphite, 0.75 for porcelain, 0.86 for Bakelite and 0.95 for plaster of Paris.[9] The samples with the crack-initiating notch were broken in shear. The fractal analysis of the profilometry data was performed using eq. (21) for the power spectrum and eq. (19) for the return probability histogram (or chord length distribution). The analyzed profiles were recorded in steps of 25 μm on a total length comprising of 256 steps. The two methods produced roughly similar results with an estimated accuracy of 10% in each case. The linear part of the logarithmic plot of the power spectrum was significantly longer than that of the return probability histogram. In fact for some materials the return probability histogram implied scaling on less than one decade. We will return below to the issue of the range of scales over which the fracture surface is expected to be fractal.

Brandt and Prokopski[52] studied Mode II fracture of a family of concretes and analyzed the profile length scaling using the vertical sectioning method applied to surface replicas. They found $H = 0.95 \pm 0.01$ from the scaling analysis in the ruler length from 30 to 500 μm. Within this narrow interval for H there was found a trend towards higher fractal dimension for specimens with higher fracture toughness. The slightly lower value of $H = 0.91 \pm 0.02$ is given by Saouma *et al.*[53] for a number of ordinary concretes fractured in uniaxial compression. These authors did not find any correlation between D and material properties.

Kumar *et al.*[54] presented results on power spectrum analysis of *in situ* apertures of intact rock fractures. The aperture profile was determined as a difference between the profiles of two walls separated by the crack. The scaling was observed over nearly two decades and it is characterized with $H = 0.72 \pm 0.08$. However, one should keep in mind that these values are not directly comparable to other results in this review, since the rock fracture surfaces were subject to erosion next to the cracking process.

Finally we would like to mention recent results of Kertész[55] who has carried out

experimental fractal analysis of the two-dimensional fracture. His unconventional experiment involved tearing paper sheets in the standard tensile testing machine and studying the fracture lines. The width of the profile was analyzed directly, and the roughness exponent was determined using eq. (18). The resulting values of H for different types of paper were all in the range from 0.63 to 0.72 in agreement with the results of 2D modelling.[7]

3.2.2. *Metals and alloys*

Under most circumstances metals are considered to be ductile materials but they can also exhibit brittle or quasibrittle behaviour given the right conditions. In fact, a well-known phenomenon is the ductile–brittle transition observed in nearly any metal at low temperatures. This transition is caused by different temperature dependencies of the strength and the yield stress.[56] Thus it is often possible to study brittle fracture of a normally ductile metal by testing it at low temperature (e.g. by immersing the metal in liquid nitrogen). For a number of metals the value of the transition temperature, T_{db}, is higher than room temperature. The most common examples would be steel, when it is subject to corrosion, or intermetallic compounds. Brittle fracture processes in metals can be categorized by considering separately transgranular cleavage, intergranular brittle failure or quasicleavage.[14] A very important question is whether these different fracture processes can result in different roughness characteristics. For example, since one of the holy grails is to relate the roughness features to materials' properties, then dependence of the roughness features on parameters other than such properties is an extremely significant information. As we show below, the experimental accuracy is usually not sufficiently high to distinguish between the effects of the different fracture processes. Clarification of this point is further complicated by the lack of sufficient information in the literature on the mode of fracture of the material under analysis.

Dauskardt *et al.*[14] presented perhaps the best documented study of the fractal character of steel fracture surfaces under different testing conditions. They used the vertical sectioning method and eq. (5a) for the profile length scaling to find D_d. The step size was in the range from 0.7 μm to 2 mm. The results were analyzed in terms of D_d (see Section 2.2), so we have used eq. (5) to convert the values of D_d from Ref. (14) into a set of roughness exponents, H. We review now briefly the results of Dauskardt *et al.* for different modes of brittle fracture.

Transgranular cleavage was measured after impact fracturing of Charpy V-notch specimens of an AISI 1008 mild steel at the liquid nitrogen temperature. The resulting $\log L$–$\log \delta$ plot can be best described as inverse sigmoidal curve[15] though an attempt was made in that work to also represent it as two linear parts with the crossover at $\delta_0 \approx 10\ \mu$m. The main linear part at $\delta > \delta_0$ gave $H = 0.93 \pm 0.02$, and δ was in this case of the order of grain size. At smaller values of δ comparable with the distance between cleavage steps H was found to be 0.98 ± 0.02.

Fracture of a 31 wt.% Mn-steel at liquid nitrogen temperature resulted in brittle intergranular cracking. The $\log L$–$\log \delta$ plot had again an inverse sigmoidal shape which was rather optimistically interpreted as a superposition of three linear parts. These parts were characterized with values of $H = 0.79 \pm 0.02$ for $\delta > 35\ \mu$m, 0.92 ± 0.02 for intermediate values of δ, and 0.94 ± 0.02 for $\delta < 5\ \mu$m. An attempt was made to relate the different length scales to the average distance between typical structural elements, but the linear decomposition of the original plot seems to introduce too large an error to be convincing.

A case of quasicleavage mode was illustrated by Dauskardt *et al.* by fracturing a low alloy ASTM A533B steel at liquid nitrogen temperature, in as-received and hydrogen-charged conditions.[14] A pronounced linear part was found for $1\ \mu\text{m} < \delta < 100\ \mu$m with $H = 0.91 \pm 0.02$, the error refers to the difference between the uncharged and hydrogen

charged conditions. The regime $100\,\mu m < \delta < 1000\,\mu m$ was fitted with a roughness exponent of $H = 0.97 \pm 0.02$. Dauskardt *et al.* then concluded that the fractal behaviour is different on different length scales, and that the crossover point correlates with the typical microstructural parameters. This observation can be of significance in that it can potentially make a dent in the hypothesis of the existence of a universal value of H.[8] However, the experimental data in Ref. (14) can be also interpreted as a simple non-fractal behaviour. So instead of questioning universality, this may in fact call into question the very existence of scale invariance. Preliminary results suggest that studies of these surfaces using the new method suggested in Refs. (10, 11, 56) can yield some more information and may shed light on this issue.

Long *et al.*[16] studied the quasicleavage fracture mode for hydrogen charged high-strength steel $30CrMnSiNi_2A$ loaded in the cantilever bending test. The scaling of vertical profile lengths was analyzed using eq. (5) with ruler lengths from 1 to $150\,\mu m$. Again an inverse sigmoidal curve was obtained with a pronounced quasi linear central part. A linear fit of its slope gives $H = 0.91 \pm 0.01$ and this value is shown to be the same in two perpendicular directions on the surface. The profile dimensions have been measured by Long *et al.* in these two directions, $\mathbf{D}'_\perp$ and $\mathbf{D}'_\parallel$, who then proceeded to determine the surface dimension D using the doubtful expression $D = \mathbf{D}'_\perp + \mathbf{D}'_\parallel$. Since they find $\mathbf{D}'_\perp \approx \mathbf{D}'_\parallel$, their calculation gives $D = 2\mathbf{D}'$, in disagreement with Mandelbrot's rule $D = \mathbf{D}' + 1$.

The same steel in as-received state has been tested by Mu and Lung[58] using essentially the same technique as described above. They observed scaling of the profile length over 1.5 decades which corresponds to ruler lengths from 4 to $100\,\mu m$. They found slightly different values for $\mathbf{D}'$ for the profiles obtained by sectioning along the crack propagation direction and normal to it. These authors reported values of $\mathbf{D}\|$ that ranged from 1.08 to 1.15 of $\mathbf{D}'_\perp$ from 1.05 to 1.10 depending on the heat treatment. The average value of H is 0.91 ± 0.05 which agrees with the results of Ref. (16). An interesting conclusion made by Mu and Lung[58] is that the fracture surface cannot be described as an isotropic fractal in the x-y plane. The main difference between $\mathbf{D}'_\parallel$ and $\mathbf{D}'_\perp$ is not in the absolute value of these dimensions, but in their dependence on K_{IC}. In both cases this dependence can be fitted by a linear relation, but increasing for $\mathbf{D}'_\parallel$ and decreasing for $\mathbf{D}'_\perp$! This conclusion, however, is only qualitative. The range of the scaling regime and that of the fracture toughness differences were too small to produce notable systematic effect taking into account the experimental error of the measurement of $\mathbf{D}'$. To the best of our knowledge no other group has reported similar findings.

Mu *et al.*[59] have recently suggested a new technique of the fractal dimension measurement and tested it in the study of the same $30CrMnSiNi_2A$ steel fractured at low temperatures. They claim that the slit island perimeter scales with its maximum diameter as $\mathscr{P} \propto d_{max}^{\mathbf{D}'}$. The surfaces of the specimens tested in three-point bending at $-60°C$ were analyzed using both this method and the conventional perimeter-area scaling relation, eq. (24). It was found that in the limit of very small yardsticks (shorter than $1\,\mu m$) the two methods agree with each other and produce $H = 0.78 \pm 0.05$. The situation is more complicated when yardsticks in the range from 2 to $6\,\mu m$ are used. The area–perimeter scaling method gives H that grows with the yardstick length, while the scaling in logarithmic coordinates, $\log \mathscr{A}$–$\log \mathscr{P}$, deteriorates. The perimeter–diameter relation gives a yardstick-independent value of $H = 0.67$ that is substantially lower than that found with a smaller yardstick. The authors' interpretation favours the perimeter–diameter scaling as the more accurate of the two approaches. The length scale dependence of the roughness exponent is explained by the presence of the two different fractal structures. We should also note that the values of H reported in this work

are generally lower than found previously for the same material under different testing conditions.[58]

Ray and Mandal[20] investigated transgranular cleavage of structural high-strength low alloy steel (HSLA) fractured in impact tests at temperatures from -50 to $-20°C$. Both the SIM and the vertical sectioning method were used to evaluate D. The vertical sections were analyzed using eq. (5) for profile length scaling using δ in the range from 3.7 to 100 μm. The $\log L$–$\log \delta$ plots were highly non-linear for all samples displaying once again an inverse sigmoidal behaviour. A linear regression analysis gave $H = 0.96$–0.99, though the slope of the nearly linear part of the plot would produce somewhat lower values, $H = 0.96$–0.99, though the slope of the nearly linear part of the plot would produce somewhat lower values, $H = 0.90$–0.95. The SIM data were entirely misinterpreted because a wrong area–perimeter relation was used (see Section 2.3). By re-analyzing their results using eq. (24), we have found that H ranges from 0.12 to 0.67. The value of D found in Ref. (20) from SIM was observed to decrease with the increase in the fracture toughness. According to Lung and coworkers[5,23] this may indicate that the ruler lengths were too large for the SIM analysis. It should be noted that the data in the plot of $\log \mathscr{A}$ vs. $\log \mathscr{P}$ were sufficient for reasonable statistical analysis for the two samples only, with $H = 0.50$ and 0.67. Therefore, in our opinion, the SIM results in this work indicate that $H = 0.6 \pm 0.1$. In view of the low data quality any conclusion concerning correlation between D and K_{IC} could be only tentative.

Przerada and Bochneck[60] measured the fractal dimension of a low-carbon microalloyed steel 22G2B quenched at different rates and fractured in three-point bending. They used the vertical sectioning method, eq. (5), and observed scaling in the yardstick length range from 0.01 to 2 mm. The calculated roughness exponent was in the range from 0.86 to 0.95. The bainite–martensite structure was found to have higher fracture toughness and lower fractal dimension than the ferrite–pearlite–bainite mixture. No conclusions on the relation between D and J_{IC} could be drawn in view of presumably different failure mechanisms for different phase compositions.

An interesting analysis of a fracture pattern is reported by Horvath and Herrmann[60] for corrosion cracking observed in a variety of alloys including Inconel 600, Monel 400, aluminium alloy 7079-T6, ternary Al–Mg–Zn alloy. They evaluated the fractal dimension from digitized images of two-dimensional cuts through stress–corrosion cracks using a modified version of the box-counting algorithm. They have found that $H = 0.62 \pm 0.05$ describes the roughness of the cracks in all the materials that these authors have studied. This technique is not quite equivalent to the vertical sectioning of the fractured sample, as their investigation is based on cutting a sample with an already developed crack pattern, but before the final fracture event.

Krupin and Kiselev reported another study of corrosion-induced brittle intergranular cracking of HSLA steels 4130 and 4340, which were fractured at room temperature in the four-point bending test.[21,22] The vertical sectioning method for the profile length scaling (eq. (5)) gave $H = 0.84$–0.94 for 4340 steel. The conclusion reached in Ref. (21) concerning inconsistency between these values and the SIM results seems to be based on mis-interpretation of the area-perimeter relation. Using data from Ref. (21) and the correct form of eq. (24) we have concluded that in this study $H = 0.75$–0.86 for 4340 steel and $H = 0.82$–0.94 for 4130 steel. The cleavage fracture of the HSLA steel after impact test in liquid nitrogen produces $H = 0.80 \pm 0.05$.

Long *et al.*[62] studied a high-strength steel $30CrMnSiNi_2$ fractured in stress–corrosion cracking mode. We remind the reader that this technique involves cyclic bending loading applied to the specimen immersed in a corrosive environment. The environmental medium

used by Long *et al.* was distilled water. Subcritical crack propagation surface was analyzed using the vertical sectioning method and eq. (5a). The profile length was measured with ruler lengths from 1 to 100 μm. The L (δ) plot was found to be linear for approximately one decade. Different modes of fracture have been observed according to the scanning electron microscopy data, and these modes were confirmed by measurements of the stress intensity factor. They found $H = 0.92 \pm 0.02$ for the purely brittle fracture, which drops to 0.89 ± 0.02 at higher K_I when a quasicleavage fracture and microvoid coalescence become operative. It was therefore claimed that D increases with K_I. But the short length scales over which a fractal dimension could be seen is quite small. No analytical fit of the dependence of K_I on D was attempted in this case by the authors. However, trying to fit their data we find that:

$$K_{IC} \propto K_0 \exp(\beta(\mathbf{D}' - 1)), \tag{31}$$

with a positive coefficient $\beta \approx 30 \pm 6$. The high value of β simply reflects the typically small magnitude of the quantity $\mathbf{D}' - 1$ (of order 0.1). It is worth mentioning that the values of H reported by the authors agree well with the results obtained for the same steel under different fracture conditions.[16,58] This may reflect either the underlying physics of the fracture process or the limitation of the profile length analysis technique.

Fahmy *et al.*[63] investigated the correlation between the value of D and the fracture toughness of V_3Au intermetallic compound with different oxygen contents. The samples contained variable amounts of the A15 phase and of the $L'1_2$ phase, with the concentration varying over the entire range between either of them being in a single phase structure. The $L'1_2$ phase has a metal perovskite structure and is produced and stabilized from a more complex A15 structure by interstitial addition of oxygen. The A15 phase is more brittle and its value of the K_{IC} increases toughness, that was measured by an impact test at room temperature. The recording step for the analysis of the roughness was 3 μm which may have been too large for sampling grains with a typical size of 30 μm. The resulting value of H was in the range from 0.40 to 0.53 depending on the heat treatment. The accuracy of these results is rather low in view of the non-linear character of the $\log p$—$\log f$ plots.

Fractal analysis of single crystals of molybdenum[65] and chromium[66] fractured at room temperature and at -196°C has been performed using STM and SEM. STM images were recorded on a grid of 128 × 128 points with a scan length ranging from 16 nm to 8 μm. The power spectra reported for Cr surfaces[65] did not exhibit any significant scaling as one would expect for such coarse grid.[47] However, the box counting method which was applied to individual profiles produced linear plots in logarithmic coordinates with scaling observed over about two decades. The roughness scaling exponent was 0.95 ± 0.04 for both metals and depended on neither the scan range nor on the temperature of mechanical testing. The same value was found for molybdenum from analysis of a three-dimensional SEM image restored numerically from a stereo pair.[65] In the latter case the image size was up to 30 μm. The scaling behavior disappeared only when the recording step of the STM decreased to 0.125 nm, which is below the interatomic distances. Images at all scales show cleavage steps as the main structural element. These are supposedly due to crossing of screw dislocations by a crack front. In case of chromium there has been observed another family of steps created by aggregation of cracks originally propagating in different planes.[66] Surface regions with such steps were characterized by $H = 0.84$. All these results are somewhat surprising because usually 128 points are insufficient for an accurate determination of scaling. Nevertheless, in this case very consistent results were obtained confirming scaling down to separations as low as 3 Å. Also the value of the scaling exponent in nanometer region is much higher than that reported by others.[44,47,56] We strongly suspect that at least the high resolution images analyzed

in Refs (65, 66) represent noise rather than the physical profile. The STM of the type employed in this study should be used in different operating regimes (bias voltage, scan rate, tunneling current) in order to obtain images with scan sizes that differ by three orders of magnitude. From the description given by the authors we conclude that this has not been done and the same setting parameters were used in all regimes. This had to lead to an increase of the noise to signal ratio of the high resolution images.

To conclude this section, the values of H for brittle fracture surfaces have been found to span a wide range of values from 0.6 to 1.0. The value of D appears in most cases to increase with K_{IC}, more supporting than not the view that brittle materials with higher toughness tend to have more irregular fracture surfaces. It is important to note that this observation holds for values of fracture toughness that correspond only to brittle fracture. Further increase in toughness is accompanied by a change of the failure mechanism from brittle to ductile fracture (rupture). We summarize results for analyses of ductile materials in the next section.

3.3. *Ductile Fracture*

The first analysis of the roughness of a ductile fracture was carried out by Mandelbrot *et al.*,[4] who studied a fracture surface of 300 grade maraging steel. Samples were fractured in an impact test and then the surfaces were studied by vertical sectioning using eq. (16) for the integrated power spectrum, and by SIM using eq. (24). The values of H were found to range from 0.72 to 0.90, depending on the heat treatment history. In that study D was found to decrease with increasing impact energy, as opposed to its increase usually reported for brittle materials. Notice that already in that seminal work the authors mentioned the presence of several linear parts in the logarithmic plots, a phenomenon that was later observed by other groups (e.g. Refs 14, 15) and which relates to a crossover behaviour as we discuss below.

Dauskardt *et al.*[14] studied a ductile fracture mode when the rupture mechanism was via microvoid coalescence. This study was carried out on 31% Mn-steel that had undergone impact test at room temperature. The plots of $\log L$ vs. $\log \delta$ for vertical sections were found to exhibit two linear parts characterized by $H = 0.85 \pm 0.02$ and 0.94 ± 0.02 which were measured using eq. (5)

Another example of rupture has been reported in Ref. (14), where an intergranular microvoid coalescence was studied for the low alloy A533B steel after hydrogen attack at high temperature. Impact fracture in liquid nitrogen revealed microvoid dimples and bigger fissures on the grain-boundary facets. We have derived three values of H from different scaling regions in the plot of $\log L$ vs. $\log \delta$ of Ref. (14): 0.96 ± 0.02, 0.88 ± 0.02 and 0.93 ± 0.02. The corresponding linear parts reflect the presence of three microstructural elements with different typical size and spacing.

A similar method based on the vertical sectioning and profile length measurement, eq. (5), was applied to Underwood and Banerji to study the surface of fractured AISI 4340 steel after different heat treatments.[15] The resulting plots display the familiar inverse sigmoidal shape with a linear part over at least one decade, yielding $H = 0.93 \pm 0.05$. There has been found a slight indication that D increases with K_{IC}, as a drop of 0.02 in D was observed for a sample with temper brittleness (lower K_{IC} value). However, the linear fit to the curves of $\log L$ vs. $\log \delta$ does not seem to be sufficiently accurate to support this observation with confidence.

Tanaka reported results of an extensive study of correlations between creep–rupture properties of heat-resistant alloys and fracture surface roughness.[67] He measured the box dimension of profiles obtained in the vertical sectioning method by covering them with either squares or circles. For a fractal curve the number of covering elements should scale according

to eq. (2) in both cases. Experimentally Tanaka found that the square grid coverage produced a box dimension which was higher by approximately 0.1. He argues that the circle coverage is better suited for a system with the matrix–precipitate interface, although, if the scale length is sufficiently large, there is no reason why the two schemes should give results that differ by more than the error bars.

Tanaka's paper seems to present the first report on the relation between fractal properties of fracture surfaces and geometry of grain boundaries in polycrystals. Indeed if this geometry is fractal it is plausible that brittle intergranular fracture that develop along the grain boundaries would produce a surface with a similar fractal dimension. On the other hand, transgranular fracture of the same material should, in principle, result in a different surface geometry. This idea was confirmed in studies of the following alloys: Ni-based Inconel X-750 and Inconel 751, Co-based HS-21 and L-605, and a 21Cr–4Ni–9Mn steel.[67] Another set of data in this paper refers to carbon steels with the ferrite–pearlite structure. Creep–rupture tests were carried out in the temperature range from 600 to 1150°C for heat-resistant alloys and at 600°C for carbon steels. In all cases scaling was observed with linear regions in logarithmic coordinates. Unfortunately, this investigation covered a range of scales from 0.5 to 20 μm, which is too short to determine the scaling properties to a good accuracy. Therefore we tend to regard the results showing fractality of the fracture surface and the grain boundaries down to 'interatomic spacings'[67] as very tentative at best.

Heat treatment which typically increases the rupture strength of heat-resistant alloys, also introduces visually serrated, rather than straight, grain boundaries. This was manifested in an increase of D from 1.01–1.05 to 1.05–1.23. An increase of the fractal dimension with K_{IC} was also observed, but the scatter in the results of Ref. (67) is too high to justify the claimed analytical dependence of the fractal dimension on K_{IC}. The summary of the roughness exponent values for these alloys is: 0.87 ± 0.04 for 21Cr–4Ni–9Mn steel, 0.85 ± 0.04 for L605 and 0.90 ± 0.06 for HS-21, 0.93 ± 0.03 for Inconel X-750. Statistical error includes the difference between the characteristics of samples with different heat treatment history or fractured under different conditions.

Tanaka also studied the dependence of the surface structure on the volume fraction of pearlite in carbon steels containing from 0.03 to 0.83%C.[67] He carried out the analysis for grain boundaries between both similar and different phase components. The roughness exponent increases monotonously from 0.84 to 0.93 when the structure changes from ferrite to pearlite. Fracture in pearlite occurs typically intergranularly, and indeed the fractal dimension of the surface follows closely that of the grain boundaries. The fracture surfaces of low-carbon ferritic steels, on the other hand, are characterized by values of D that are 0.10–0.12 higher than for the ferrite–ferrite boundaries and only 0.02–0.06 higher than for the pearlite-ferrite boundaries. These results are consistent with the observed ductile fracture accompanied by substantial plastic deformation in the case of ferritic steels, and with quasi-brittle intergranular fracture of perlitic steels. Such a combined analysis of grain boundaries and of the fracture surface supplements successfully traditional qualitative description of different modes of fracture.[14,55]

Lung and Zhang carried out three-point bending tests at temperatures in the range from 0 to -80°C in order to study fractal properties of the fractal surface of a low alloy 30CrMnSiNi$_2$ steel.[23] SIM results were analyzed using eq. (2.24) for the perimeter–area scaling with the ruler length between 0.08 and 1.85 μm. For δ in the short range they reported a value of H from 0.88 to 0.92. For higher values of δ that were comparable to those that had been used by Mandelbrot *et al.*,[4] the corresponding values of H lie in the range from 0.82 to 0.89. It is rather puzzling that in the latter case they also found a decreasing relation

between D and K_{IC} of the form (3.2) with $\beta < 0$, while for δ in the short range they found the opposite trend. This may suggest that size effects play a crucial role in this study, and the SIM analysis was probably carried out with an inappropriate choice of the ruler length.

Wang *et al.* reported a non-standard application of the SIM to analysis of the fracture surface of dual-phase ferritic–martensitic steel.[68] Fatigue tests at room temperature were carried out on notched samples, and the fractal dimension was evaluated using the perimeter–area scaling in SIM, eq. (24). The authors chose to study 'lakes within islands' pattern rather than the usual choice, 'islands within lakes'.[4] As we discussed in Section 2 the above two choices may not be equivalent for ductile fractures. Wang *et al.* found that the exponent H lies between 0.78 and 0.91, and that it depends on the volume fraction of the martensite. This significant systematic variation of D with concentration may present one of the clearest evidences for the nonuniversal nature of H. An increasing linear relation was found between D and ΔK_{th}, the fatigue threshold of the form

$$\Delta K_{th} = \Delta K_0 + \alpha(\mathbf{D}' - 1),$$

with $\alpha = 68.0$ MPa m$^{1/2}$.

The particular choice of the object for SIM analysis could affect the result significantly as illustrated by the investigation of Huang *et al.*[25] They used the impact test at room temperature to fracture samples of CK45 steel that had been tempered at different temperatures. Equation (24) was used for both possible interpretations of the coastline. In addition they determined D_d using eq. (5) for profiles recorded using the secondary electron line scanning and by the vertical sectioning. A linear relation between D and toughness was found for both choices of the object in the SIM analysis with slopes that were nearly the same in absolute value. However, the sign was positive for the standard choice, 'islands within lakes', and negative for the opposite choice. The values of H for the two cases were 0.61–0.67 and 0.73–0.78, respectively.[25] Although Huang *et al.* presented a reasonable explanation for their observations, we think that in the case of microvoid coalescence one should still use the standard interpretation for analyzing the correlations between D and toughness because it should coincide with that given by the vertical sectioning technique.[25,26] The values of H that Huang *et al.* found using eq. (5) for the profile length measurement differed significantly from the SIM data. The value of H was 0.77–0.85 from the SEM scanning and 0.87–0.91 from the vertical sectioning. However, the detailed analysis of the SEM data shows that the scan lines are extremely sensitive to the experimental details, and extreme caution should be exercised before one can claim that the scans represent the true profiles.[26]

The latter values obtained from the vertical sectioning are in reasonable agreement with the results from analysis of the fracture surface of an essentially similar carbon steel, DIN C45, which was carried out by Imre *et al.* using the electrochemical method.[31] Details of this measurement technique are given in Section 2.4. Gold replicas of an impact-fractured steel samples were prepared and the time dependence of the Faradaic current was recorded. The logarithmic plot I vs. t was found to be linear over an interval that corresponds to a ruler length between 5 and 100 μm. Using eq. (27) the value of H was estimated to be 0.85 ± 0.04. The corresponding value of D decreased slightly with increasing impact energy, but this effect was statistically insignificant. More remarkably, different values of H were claimed to have been found for different parts of the fracture surface, a phenomenon that is more common for brittle rather than ductile fracture.

We should comment that the electrochemical method used in Ref. (31) has a significant disadvantage for fractal analysis because it relies on preparing a replica ('cast') of the rough surface. This effectively cuts off the lowest scale range of the fractal behaviour due to the

inability to press into the smallest and most irregular crevices. Since the interval of length scales is crucial for these studies this inevitably reduces the accuracy of the measured exponent. In addition to reducing the accuracy, this method can bias the results for H towards lower values (smoother surfaces).

McAnulty *et al.*[69] presented evidence that, contrary to the results of Ref. (25), the choice of interpretation of either lakes within islands or islands within lakes for SIM analysis need not necessarily result in different scaling behaviour. They studied high strength and high-toughness ASTM A723 (modified AISI 4340 with 0.2% V) steel fractured in the Charpy impact test and in a low-cycle fatigue test. Perimeter–area scaling was analyzed for SIM images, using both interpretations for the fatigue fracture and only islands for the impact fracture. These two kinds of fracture were studied on different length scales, from 0.01 to 1 mm for the Charpy test and from 0.2 to 20 mm for the fatigue fracture. The scale difference implies that the two analyses pertain to regions at different distances from the initiating crack. These differences add up to paint a rather clear picture regarding the universality hypothesis in these materials, namely, different parts of the fracture surface and different length scales lead to different types of fracture. Not surprisingly, the roughness exponent is also different: 0.75 ± 0.05 for the impact fracture and 0.61 ± 0.02 for low-cycle fatigue. It is interesting that analysis of either islands and lakes interpretation yields the same results to within the statistical error.

McAnulty *et al.* tried to use a new method within the SIM context.[69] They analyzed the size distribution of the resulting islands and lakes. Mandelbrot[1] discussed this distribution in the context of geographical islands and suggested that for fractal structure this distribution should decay algebraically, $N(a) \propto a^{\mathbf{D}''/2}$, where N is the number of islands of area greater than a. The value of $\mathbf{D}''$ need not coincide with the coastline dimension $\mathbf{D}'$ for a multiconnected structure. McAnulty *et al.* have found that for fatigue fracture: (i) algebraic distribution is approximately valid for both lakes within islands and vice versa, and (ii) the numerical values of $\mathbf{D}'$ and $\mathbf{D}''$ coincide for lakes within islands and differ by only 10% for islands within lakes. Their data suggest though that the values of $\mathbf{D}'$ obtained using eq. (24) are more accurate because they are based on scaling over 3–4 decades in area, while the scaling of the algebraic distribution spans less than two decades.

Krupin and Kiselev analyzed Armco-Fe samples fractured in an impact test at different temperatures using SIM.[22] As we mentioned already the authors used the area–perimeter relation but unfortunately with a wrong expression for D. Recalculating from their data and using eq. (24), we obtain $H = 0.94$ and 0.90 for the ductile fracture at room temperature and in liquid nitrogen, respectively. The mixed fracture mode gives $H = 0.90$–0.98.

An unusually large interval of the values of H is reported by Su *et al.* for fracture surface of dual-phase ferritic-martensitic steels quenched from different annealing temperatures and subjected to impact testing at $-25°C$.[70] These authors used SIM and eq. (2.24) for the perimeter–area scaling, using a ruler length of 0.59 μm. An exponentially decreasing relation of the form of eq. (31) was found between the impact toughness, J, and the fractal dimension D, with $\beta = -0.67$. The value of H was found to drop from 0.8 to 0.22 (!) as the ferrite contents decreases.

Shibayanagi *et al.* applied the vertical sectioning method to study a Cu–9.7% Zn alloy fractured in tensile test at temperatures from 20 to 700°C.[71] The divider dimension was estimated from the scaling of the number of dividers, $N(\delta) = L(\delta)/\delta$, with the ruler length, δ. The scaling parameter, H, is then given by eq. (5b). Usually two straight parts were observed in the $\log N$ vs. $\log \delta$ plot, and the crossover point was associated with the typical size and spacing between the dimples observed on grain boundaries due to void formation.

However, the difference between the corresponding slopes, 0.90 ± 0.05 and 0.92 ± 0.05, is well within the noise level.

A simplified method to analyze the fractal structure of the dimple patterns of ductile fracture surfaces has been applied by Ishikawa to Fe–Ni alloy broken at 4 K.[72] Assuming that the dimples are circular he analyzed their size distribution using metallographic images of the surface. Scaling behaviour was observed for diameters from 1 to 50 μm with a roughness exponent of $H = 0.5$, which suggests that these are Brownian surfaces.

Jiang *et al.*[73] attempted derivation of the theoretical formula connecting the fractal dimension and the toughness J_{IC} of ductile materials. They followed Thompson and Ashby[74] in using the aspect ratio of the dimples on the surface, $M = h/w$, as the only descriptor of the surface morphology (here h and w are the dimple height and diameter, respectively). Jiang *et al.* further used the conclusion from Ref. (74) that the toughness increases as $\ln M$ and then tried to relate M to the fractal characteristics of the surface. In our opinion, the numerical relation between M and D suggested in Ref. (73) is not reliable in view of multiple uncontrollable approximations made by the authors. As a result, according to Ref. (73) the value of M lies between 0 and 0.5 for $\mathbf{D}'$ ranging from 1 to 2. The upper limit on M becomes 0.3 for the typical values of $\mathbf{D}'$ reported in the literature. At the same time Thompson and Ashby have reported experimental results on M being between 0.5 and 1.0, and there is no physical reason prohibiting the case of $M \geqslant 1$. Furthermore, the analytic relationship between J_{IC} and D derived in Ref. (73) predicts negative toughness unless the volume fraction of the void nuclei is well below 1%. The dependence deduced in Ref. (73) cannot be reconciled with the empirical relations that were used successfully to fit the experimental results, see previous section.

The experimental data by Jiang *et al.*[73] refer to the vertical sectioning study of the fracture surfaces of AISI 310 stable austenitic stainless steel. The profile length for as-received and hydrogen-charged notched specimens fractured in tensile test was analyzed using eq. (5). Scaling was studied (and found) within one decade only, thus rendering all conclusions to be only qualitative. The roughness exponent was 0.85 for the uncharged specimen and slightly higher, 0.91, for the quasi-brittle fracture of the charged one.

Bouchaud *et al.* studied a set of samples of 7475 aluminium alloy undergone different heat treatment, which were fractured in tensile test.[9,13] Two different ductile fracture processes were observed, transgranular rupture with formation of voids on the boundaries of the grains, and ductile intergranular rupture. The SIM technique was used and a two-dimensional correlation function was evaluated for digitized images of islands. The authors used a somewhat different version of the two-point correlation function by correlating points on the perimeters of the resulting islands over the entire image. This correlation function appears to give a scaling regime that is longer than two decades and therefore makes this technique one of the best among those involving two-points correlations. The value of H that they have found was 0.80 ± 0.03 irrespective of the rupture mode or fracture toughness. The latter result, however, should not be surprising since K_{IC} varies very little from sample to sample in that study. Usually K_{IC} has to span at least one order of magnitude in order to give a detectable systematic change of the fractal dimension.[4,20,63,70]

Analysis of different aluminium alloys reinforced with particulate SiC and fractured in the fatigue test has been reported by Davidson.[75] Digitized photographs of vertical sections were used to find D_d using eq. (5). The value of H was found to be 0.86 ± 0.07 in agreement with other results for Al alloys.[9] No correlation was found in Ref. (75) between D and the fracture toughness. This is probably due to the participation of several fracture mechanisms in composites, namely, crack growth, plastic deformation and void formation.

Three different methods of fractal analysis were used by Pande *et al.* to study fracture surface of a titanium 6211 (Ti–6Al–2Nb–1Ta–0.8Mo) undergone tensile testing.[12] The vertical sectioning method gave $H = 0.85 \pm 0.02$ from eq. (5). The SEM line scan produced profiles with a similar value of $H = 0.85 \pm 0.05$ (the same profile length analysis, eq. (5)). The area–perimeter relation of the SIM, eq (24), gave $H = 0.68 \pm 0.05$ in clear disagreement with the other two methods. The $\log \mathscr{A}$–$\log \mathscr{P}$ was also much less linear than in other studies, casting doubts on this low value and perhaps pointing towards an unfortunate choice of the ruler length.

Pande *et al.* studied in Ref. (76) two titanium alloys, one of them again a 6211 alloy, in a tensile test. The fractal dimension was found from vertical sectioning, eq. (5), and from SIM analysis. The $\log L$–$\log \delta$ plots were nonlinear for all samples. Instead of describing the curves as a combination of linear parts in the spirit of Ref. (14), Pande *et al.* tried to fit them with parabolic forms or with arcs of circles.[76] The authors give no explanation for this choice, and the lack of any clue regarding how they arrived at the value of $H = 0.93 \pm 0.04$ from such quadratic fits casts in our opinion strong doubts on the accuracy of this value. Also, the paper does not make it clear what analytical relationship was used for the area–perimeter analysis in SIM. The authors refer to Ref. (4) when they report their method of analysis, but, as mentioned above, eq. (24) was given there in a wrong form. To clarify this we have used their plots of $\log \mathscr{A}$ vs. $\log \mathscr{P}$ to estimate H and we have found $H = 0.99 \pm 0.03$, consistent with $H = 1$. In fact, for few samples the data was described with the values of $\mathbf{D}' < 1$ (or $H > 1$). The reason for these results lies probably with a non-fractal behaviour of the fracture surface. If so, this is a good illustration that the fractal description is only a hypothesis for fracture surfaces, although a popular and a viable one. Claims of fractal behaviour have been made in many inappropriate cases as described by Hornbogen.[77]

Further study of a 6211 titanium alloy has been carried out by Friel and Pande[28] using the surface area measurement with a stereographic SEM technique, see Section 2.4. The samples were fractured in tension similar to Ref. (76). Digital images were obtained at magnifications spanning two orders of magnitude in the length scale, and the surface relief was reconstructed numerically based on the optimum matching of the images constituting a stereo pair. The surface area scaling with the ruler length, $\log S$ vs. $\log \delta$, has been analyzed using both images taken at different magnifications and area calculations performed on different grids of points. The value of D was then estimated from the linear regression analysis of significantly non-linear plots. The plots could be regarded either as the intersection of linear parts or as sigmoidal curves, once more supporting our suspicion of nonfractal behaviour of the fracture surface of this material. The roughness exponent extracted from the data of Ref. (28) is 0.85 ± 0.10, where the uncertainty is due to the possible interpretation of the log–log plots as consisting of few linear parts with different slopes.

Richards and Dempsey measured the fractal dimension of the surface of another titanium alloy fractured in a tensile test after different heat treatments.[19] Again the wrong form of eq. (24) for $\log \mathscr{A}$ vs. $\log \mathscr{P}$ was used to estimate D from the SIM data. Using the proper relation we find from the data given in Ref. (19) that $H = 0.92 \pm 0.03$. The authors observed no correlation between D and neither tensile properties nor structural features. Since the samples did not differ in their toughness significantly, one would not expect any pronounced correlation to be found anyway.

STM topographic analysis of polycrystalline copper fatigued in compression was reported by Mitchell and Bonnell.[47] They used. eq. (16) to determine H from the integrated power spectrum and found $H = 0.61 \pm 0.04$. This value is lower than the typical results obtained on a micron-scale. But as we mentioned already in Section 3.2.1, there is an unexplained

discrepancy in their results between the scaling behaviour of $p(f)$ and $P(f)$. Hence one should be cautious in accepting their numerical estimates.

An application of STM to fractal analysis of steel fracture surfaces is presented by Denley[27] following the method of the area analysis described in Section 2.4. Neither microstructural information nor testing details were given in this paper. The analysis gave $H = 0.93 \pm 0.10$ for two fractured steel surfaces (both brittle and ductile). The accuracy of the measurement still leaves much to be desired, with the main problem being the lack of pronounced linearity in the plot of $\log S$ vs. $\log \delta$. This could be due to two reasons: (i) the grid of 400×400 pixels is not fine enough for calculations with high δ;[47] (ii) this plot exhibits an inverse sigmoidal shape as do the majority of the $\log L$–$\log \delta$ curves.

Jiang *et al.*[78] have applied the vertical section method to the study of fracture surfaces of 7475 Al alloy after superplastic deformation. The physical picture of material failure is very different in this case from the mechanisms discussed above. The superplasticity effect is achieved via accommodation of the plastic deformation in the rotation of grains with respect to each other accompanied by their elongation. This process results in the deformation values of few thousand percent. During the deformation, however, the creation of cavities between grains occurs inevitably. Thus the failure is due to their nucleation, growth and interlinkage, and the vertical section of the fractured specimen is the section through such cavities. As a result the profile is not a single-valued function, and the images are qualitatively similar to those recorded in the case of crack-branching in brittle materials[12] despite the very different underlying physics. Jiang *et al.*[78] calculated the fractal dimension using eq. (5a) for the profile length scaling which does not seem to be the best way to describe a curve with multiple overhangs. They found the values of H in the range from 0.73 to 0.89 depending on the deformation conditions. The scaling was established in a relatively wide interval of the ruler lengths, from 0.5 to 60 μm. Their data suggest that the superplastic elongation increases nearly linearly with D.

To summarize this section, there is a strong evidence that the fracture surface is self-affine for a variety of materials and models of fracture. The roughness exponent H ranges in the literature from 0.6 to 1.0 for either brittle or ductile fracture mode. When comparing results obtained by different methods, one should use the *proper relation* between D and H, namely eq. (5b) or eq. (12b). We have reviewed many of the relevant reports and pointed out the degree of reliability of different techniques. It is inherent in the problem that it is difficult to find a reasonably long linear part in the plot of $\log L$ vs. $\log \delta$. Namely, a scaling regime that spans more than two decades in length is rarely recorded experimentally. In our opinion the spectral analysis appears to be a somewhat better technique for vertical sectioning than the profile length measurement. However, the horizontal sectioning combined with analysis by SIM is in our view the most reliable method and its only drawback pertains to the choice of the image as islands or lakes in the perimeter–area analysis. Nevertheless, in many cases all these methods agree within the experimental accuracy.

The profile length analysis carried out using eq. (5) deserves special attention. Reviewing all the results obtained using this method, we find that the measured value of H rarely falls below 0.85 irrespective of the method of the profile recording, the fracture mode and/or material properties. A marked difference appears between values of H obtained from scaling of $L(\delta)$ and from any other method. An averaging over all the reports using the former gives $H = 0.91 \pm 0.04$, while an average of the results produced by all other methods gives 0.8 ± 0.1. In general all the low values of H reported so far originate from SIM, power spectrum and variation method analyses. This may also be related to the fact that the profile length scaling is usually the least linear in logarithmic coordinates. The resulting plot is either

inverse sigmoidal[15,16,20] or quadratic,[76] which is very similar to a crossover behaviour.[4,14] Therefore this method produces plots that (i) are difficult for interpretation, and (ii) result in overestimated roughness exponent. These conclusions seem to hold also for the three-dimensional generalization of the method.[27,28] In light of the usually short scaling regimes and the scatter in data, multifractal analyses seem to be out of the question for fracture surfaces in general.

One of the main purposes of this review is to address the crucial question whether there is a correlation between D and the properties of the material. Our review suggests that this is indeed so and that the nature of the correlations depend on the fracture mode. An increasing relation between fracture toughness and D has been found in all cases of brittle fracture, although the scatter in the data does not allow one to find a universal analytical expression that can fit all measurements. Linear, square root and exponential fits were attempted with varying degrees of success. One can, however, come across both increasing and decreasing such relations for ductile rupture. In some cases the decreasing relation is an artifact of an inappropriately high value of the ruler length used in the SIM.

We should also note that due to the relatively short linear regimes in the log–log plots in the above studies, they can at most indicate self-affinity of the fracture surface rather than confirm such a behaviour. Although this assumption does not appear out of place in most cases, there exist few cases where the claim of fractality is not supported by the experimental data from which the results are derived. This points to a serious and inherent problem regarding the interpretation of the fracture surface as self-affine. The large body of work into general fractal systems led to a rule of thumb, which places existence of *at least two decades* of linearity in log–log plots as a threshold that establishes scaling. Even disregarding the scatter in the values obtained for H in the studies that we have reviewed here, the measurements in the micron regime show *at best* two decades of scaling, and often less than that, thus supporting only marginally the scaling hypothesis. This suggests that the actual physics of fracture is different within the length scale range from 1 to 100 μm and outside this range. This can be due to either different governing fracture mechanisms or to different microstructural characteristics of the material on these length scales. Moreover, the crossover length scales given above seem to depend also on the material and fracture type. Thus we are confronted with a unique situation of a possible scaling on a rather narrow range of length scales between 10^{-6} and 10^{-4} m. This observation may account for the large scatter in H, as well as for the origin for many of the controversies. This explanation also sheds new light on claims of universality in roughness of fracture surfaces. First, it is difficult to define universality in such a narrow window. Second, even accepting that universality can be appropriately defined in such a window, it is difficult to define the upper and lower boundaries of the interval and to agree on what determines the location of these boundaries. The resolution of this question must be related to some physical mechanism and therefore to specific material properties.

Acceptance of this view suggests that we should look for materials that permit a wider window for scaling in order to understand the fractal geometry of fracture surfaces. The difference in the scaling of roughness at the length scale below the window is illustrated by STM analysis on the nanometer scale. This gives H that is consistently lower than that in the mesoscopic range. For example, values of 0.6 ± 0.1 for the brittle MgO,[44] 0.61 ± 0.04 for ductile copper[47] or 0.43 for carbon[18] are well outside the error margin for studies on the micron-scale for similar materials.

In view of these many technical and inherent difficulties it is reasonable to suggest a new approach, orthogonal to those used in the literature. The main aim of these studies is

ultimately to relate the morphology of the fracture surface to the mechanical properties of the material. This review shows that the roughness exponent H and the fractal dimensions are not good indicators due to their wide scatter. Therefore we search for a new descriptor that can characterize the structure independently of these exponents.

In the next two sections we give a detailed account of such a scheme. In our approach we employ a new method of analysis of scale invariant structures that is essentially an adaptation of a morphological correlator developed recently in Ref. (10) to the study of fractures.

4. A Correlator for Scale Invariant Structures

The issue of characterizing fracture structures suffers from two inherent problems, as we have already mentioned: One is the limited range of scales over which scale-invariance seems to exist, and the other is the large scatter in the values of H and D. The latter is a severe handicap because, as we have shown in Section 3, in many cases different fracture mechanisms produce qualitatively different surfaces, which happen to have a similar D. Therefore one cannot expect D to suffice for characterization of the structure of the surface. This reasoning alone already suggests that attempts to relate D to material properties may be doomed to failure. All the above techniques of analysis, as well as the presently existing methods of fractal analysis in general, suffer from a fundamental conceptual limitation: they all rely solely on information from *two-point correlations* in the system. The pair correlation function $G(x)$ and the corresponding Fourier spectrum, described in Section 2.2.2, scale with an exponent that depends linearly on D. Quite generally, any probe that relates to the two-point correlation function can at most reveal the fractal dimension (or some other exponent linearly-dependent on it) and nothing more. The value of H (or D) has been indeed the goal in all the methods that we have reviewed. Therefore for a new approach to be useful it should address these limitations and hopefully improve on existing techniques in these aspects.

Such a method has been recently outlined by Blumenfeld and Ball.[10,11] The derivation there was given in terms of mass fractals and density–density correlations. We can conform to those notations by establishing correspondence between the one-dimensional profile, $h(x)$, and the distribution of a measure, $M(x) = h^2(x)$. The square of the height is used so that we treat a non-negative quantity. Given a data set on a one-dimensional grid we choose a grid point, which we index as i, and construct concentric shells around it. The shells are chosen to have a uniform width in *logarithm* of the distance r from i. Defining $\rho = \log r/\log 2$, we measure for each point i the mass, $\delta S_i(\rho)$, in a spherical shell at the radius ρ from it. The average of $\delta S_i(\rho)$ over all choices of i is proportional to the traditional pair correlation function that gives the mean mass in a shell, but is a function of ρ instead of the usual r.

We define now the relative fluctuations in the distribution of the measure (mass) about point i in terms of the relative shell masses,

$$\delta\sigma_i = \frac{\delta S_i(\rho)}{\langle \delta S(\rho) \rangle}, \tag{32}$$

where the angular brackets, $\langle\ \rangle$, stand for an average over all possible origins i. Statistics of a self-similar fractal are invariant under dilational transformation $\mathbf{r} \to \mathbf{r}' = \lambda \mathbf{r}$. Therefore, by working in ρ-space we reduce the symmetry to translational invariance, namely, invariance under $\rho \to \rho' = \rho + \ln\lambda$. It follows: (i) that correlations of $\delta\sigma_i$ in such structures, which are on *multiplicative* scales, can be treated with traditional tools in ρ-space, and (ii) that insight from decades of analysis of translational invariant systems can be applied to the present

analysis. A significant quantity that Blumenfeld and Ball[10] have introduced is the correlation matrix,

$$M(\rho, \rho') = \langle \delta\sigma_i(\rho)\delta\sigma_i(\rho') \rangle, \tag{33}$$

which was anticipated to be overall scale-invariant, namely, $M(\rho, \rho')\mathrm{p} \propto \mathscr{L}(\rho - \rho')$. This form is equivalent to the three-point correlation function of the system in ρ-space. Thus defined the function $\mathscr{L}$ represents an average of relative shell masses. This formulation is straightforward to generalize for objects embedded in higher Euclidean dimensions.[10] For later use we rewrite eq. (33) in a form modified to analyze surfaces:[53]

$$M(\rho, \rho') = \frac{\langle [h(\mathbf{r}_1) - h(\mathbf{r}_2)]^2 [h(\mathbf{r}_1) - h(\mathbf{r}_3)]^2 \rangle_{|\mathbf{r}_1 - \mathbf{r}_2| = 2^\rho; |\mathbf{r}_1 - \mathbf{r}_3| = 2^{\rho'}}}{\langle [h(\mathbf{r}_1) - h(\mathbf{r}_2)]^2 \rangle_{|\mathbf{r}_1 - \mathbf{r}_2| = 2^\rho} \langle [h(\mathbf{r}_1) - h(\mathbf{r}_3)]^2 \rangle_{|\mathbf{r}_1 - \mathbf{r}_3| = 2^{\rho'}}}. \tag{34}$$

Several two-dimensional isotropic and fractal systems were generated numerically and studied in Ref. (10), using this method: a 4000-monomer-long self-avoiding walk, a 4096 particle cluster-cluster aggregate, a sample of 10^4 particles chosen randomly from a 10^5-particle diffusion-limited aggregate, and disordered Cantor sets. Two main conclusions should be mentioned: (i) The correlation matrix of a scale-invariant system should exhibit lines parallel to the diagonal. This follows from the fact that correlations in such system must depend only on relative separation $|\rho - \rho'|$ and represents a fingerprint of a fractal structure; (ii) The corresponding functions $\mathscr{L}$ show nontrivial features that yield information on the structure of the system. Typically $\mathscr{L}$ starts from a value larger than one, and decreases to eventually saturate to unity for $|\rho - \rho'|$ larger than some characteristic value λ_s. This means that when $r'/r > \exp(\lambda_s)$ subsets of the structure on different scales are uncorrelated. The values of λ_s, as well as the detailed behaviour of $\mathscr{L}$ for $|\rho - \rho'| < \lambda_s$, were found to differ from system to system, even though some examples were constructed to have very similar fractal dimensions. Thus M and $\mathscr{L}$ provide an analytic tool to distinguish between different signatures of fractal patterns with similar values of D.

Therefore this description seems to overcome all three difficulties mentioned above: (i) It can confirm existence of scale-invariance by inspection of M; (ii) It is sensitive to the signature of the fractal structure beyond the fractal dimension; (iii) It reveals information that is unattainable by a two-point correlation function.

5. STM Study of Fracture Surfaces

The scanning tunneling microscopy (STM) was invented primarily as an instrument for high resolution study of surface structure on atomic level.[79] However, its operational simplicity made it a popular tool for investigations on the micron scale, which is a low resolution regime of the STM.[80] STM is an attractive method for fractal analysis at the lower limit of the roughness length scale because the surface images are conveniently recorded in a digital form.[27,44,47] This technique also enjoys the advantage of being nondestructive since no sample sectioning is involved. Moreover, STM does not require as extensive a sample preparation as vertical sectioning or SIM techniques.

The price to pay for these attractive features is relatively low. First, there is a fundamental problem of the image being a convolution of the true profile with the shape of the tip. If there are sharp protrusions on the surface then the recorded image represents multiple tip images rather than a picture of the surface.[80,81] Such a situation is rather improbable for fracture surfaces, but there exists the possibility that the spectrum of the profile can be distorted as

a result of convolution. This effect would not be present for an ideally sharp tip. For reasonably sharp tips that allow reproducible and reliable imaging the convolution is believed to be an insignificant source of error.[47] An error is also introduced due to the unavoidable noise in both scanning and recording circuits. This noise and its influence on the results can be analyzed quantitatively, see Ref. (47) and below. Another problem of STM is that the standard equipment allows maximal lateral displacement of the tip of order of 10 μm only, thus the length scale over which the analysis is carried out is necessarily different than that used by other methods. However, it is possible to build an STM that combines usual high resolution scanning with a coarse drive capable of scanning over the 20 mm $\times$ 20 mm area.[82] The first application of such device to the problem of the crack opening in brittle materials shows its great capacity for the analysis of fracture surfaces.[82] Scanning within the limits given above with scanning steps from 50 to 500 nm[82] would be very useful in producing images most suitable for the analysis of fracture surfaces.

We use STM here to address the following issues: (i) Is the fractal description applicable to cleaved fracture surfaces down to nanometer scales? and (ii) Can we probe the difference in scaling behaviour of surface regions with different roughness (mirror, mist, crack branching zone). For completeness, we use both traditional methods of fractal analysis, Sections 2.2.2 and 2.2.3, as well as the correlation scheme outlined in Section 4.

FIG. 1(a).

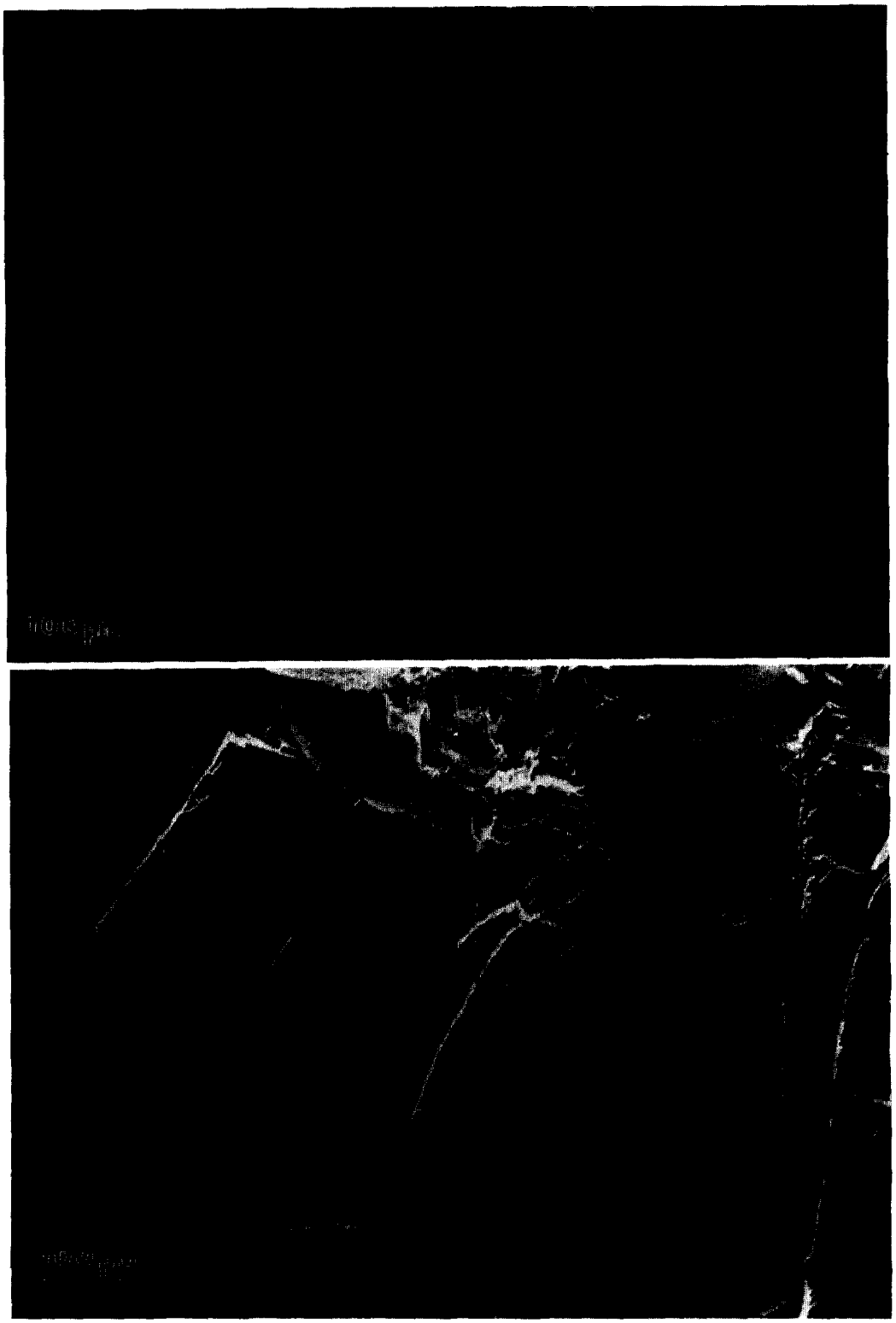

FIG. 1(b,c).

FIG. 1. SEM images of the tungsten cleavage surface: (a,b) backscattered electrons; (c) secondary electrons.

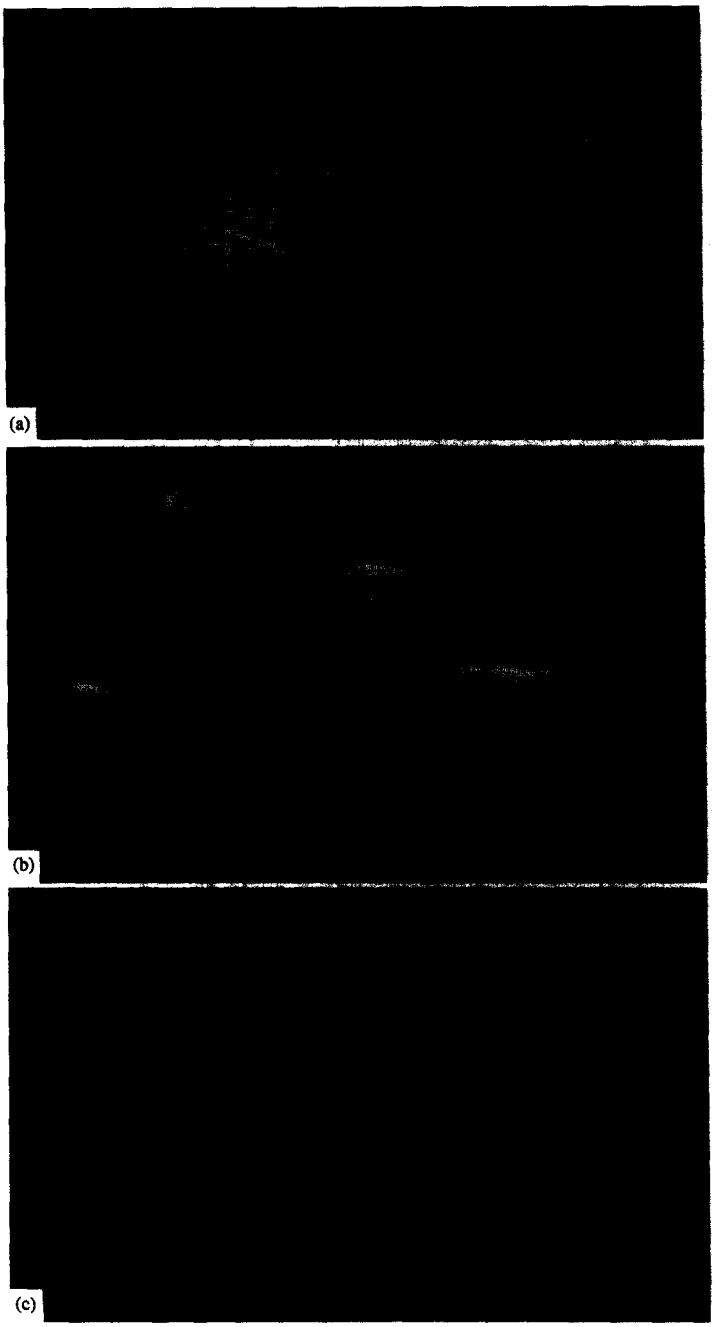

FIG. 2(a–c).

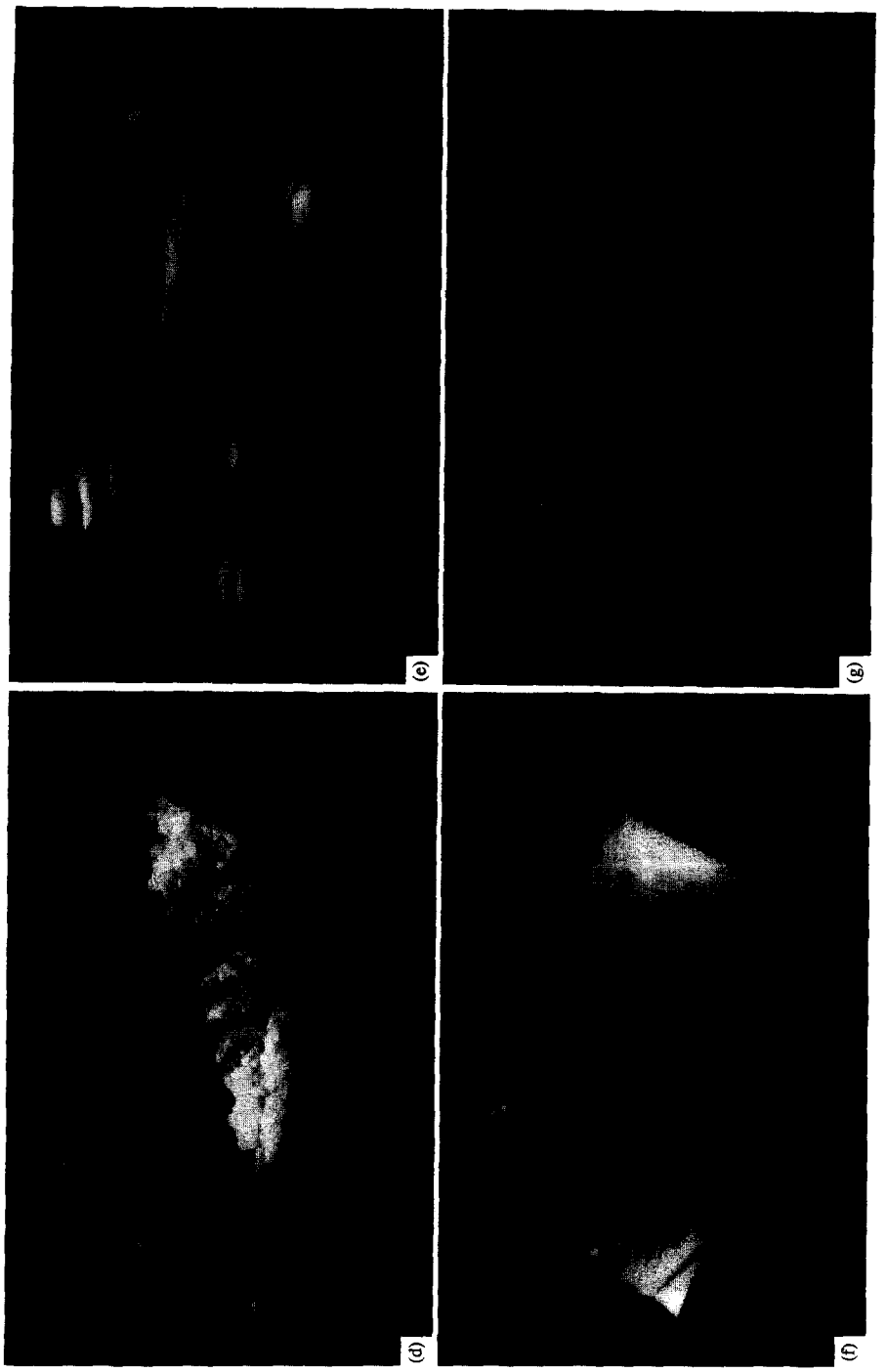

FIG. 2(d–g).

FIG. 2. STM images of fracture surfaces: (a) tungsten, 'mirror' (500 mV, 1 nA); (b, c) tungsten, stepped 'mist' at different magnifications (500 mV, 1 nA and − 300 mV, 1 nA, correspondingly); (d, e) tungsten, stepped crack branching region (300 mV, 1 nA); (f, g) graphite at different magnifications (20 mV, 2 nA).

5.1. *Experimental Details*

Brittle fracture surfaces of pure tungsten single crystals were prepared by impact fracture of notched samples cooled in liquid nitrogen. The SEM micrograph of a typical (001) cleavage surface clearly shows a flat mirror region followed by a mist and a microcrack branching zone, Fig. 1. An interesting feature is a set of parallel steps in the mist zone. We carried out separate analyses for these three regions. We studied also the (0001) surface of the highly oriented pyrolithic graphite (HOPG) obtained by exfoliation (pencil glide).

The constant current images were recorded in a 400 × 400 pixel format using commercial STM operating in air.[83] We studied images at two magnifications with scan length of 7140 nm (the maximum scan size of the specific STM that we used) and of 714 nm. Therefore we covered more than three orders of magnitude in lateral separation with the shortest sampling step being 1.8 nm. Images were obtained with a tungsten tip at sample bias of 20 mV and

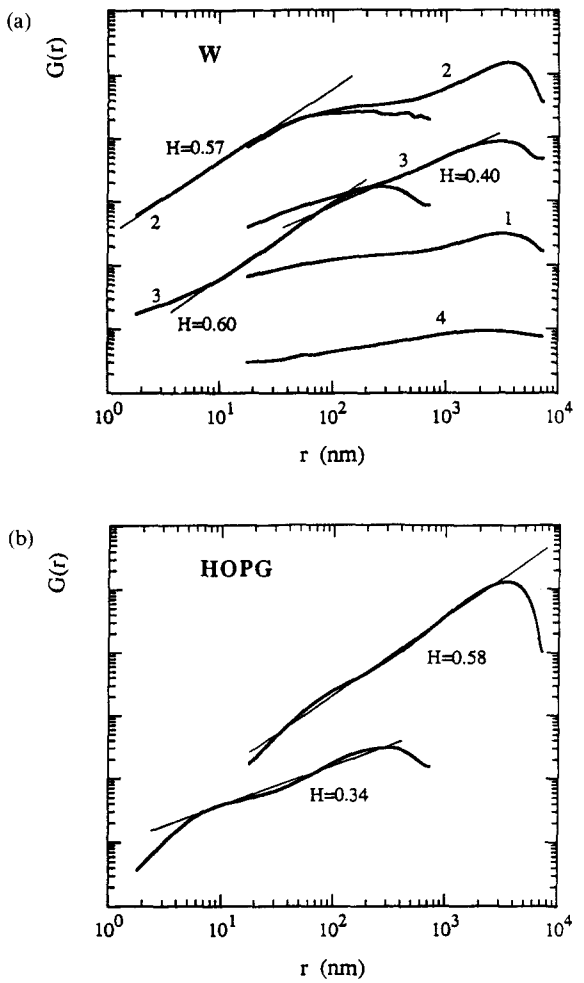

FIG. 3. The pair correlation function, $G(x)$: (a) tungsten fracture surface; 1—mirror, 2—crack branching region, 3—mist, 4—noise signal acquired at 300 mV, 1 nA; (b) graphite fracture surface.

tunneling current of 2 nA for graphite, and either +500 or −300 mV bias and 1 nA current for tungsten. The only post-acquisition filtering was the subtraction of the least-squares fitted plane from all images. Representative examples of the surface morphology are shown in Fig. 2.

The issue of the statistical reliability of STM data for fractal analysis was discussed in Ref. (47). The main points of concern are the number of sampling points and the noise to signal ratio, and it is therefore best to use profiles containing at least 1000 pixels. Unfortunately, to the best of our knowledge, such an option is not available on any commercial STM.[79] We monitored the noise level in the image using the method similar to

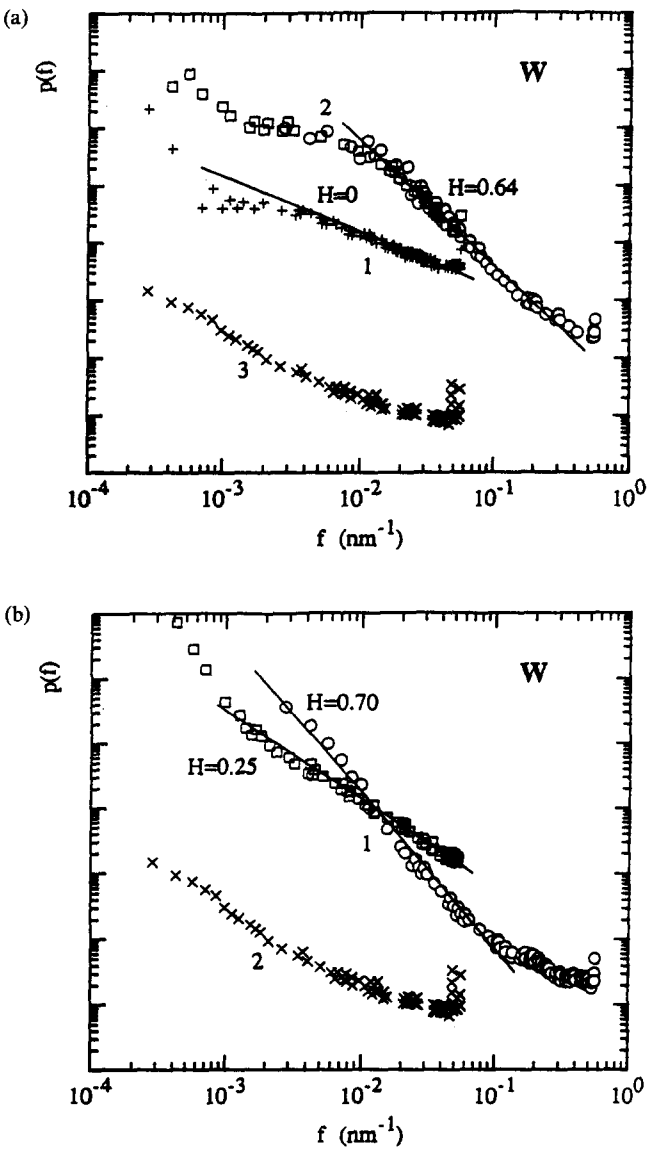

FIG. 4(a,b).

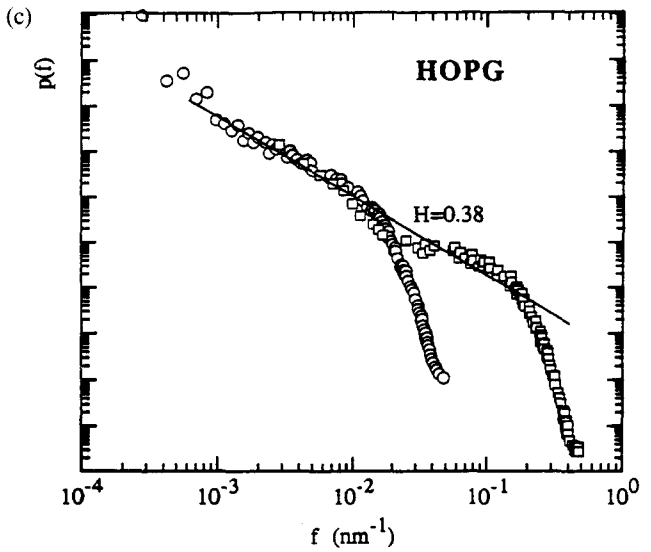

FIG. 4(c).

FIG. 4. The power spectrum, $p(f)$: (a) tungsten; 1—mirror, 2—crack branching, 3—noise; (b) tungsten; 1—mist, 2—noise; (c) graphite.

that described in Ref. (47). The signal due to sample drift and due to the noise in the voltage amplifiers was obtained with an immobile tip. All STM parameters were adjusted as for proper scanning, and the resulting image was recorded in the standard STM format. For the purpose of the analysis we treated these 'noise images' as real images and consequently we discarded those STM pictures for which the ratio of the signal power spectrum to the spectrum of the noise image was less than 100. The images taken at a small scan size (70 or 35 nm) were noisier than those shown in Fig. 2, and therefore could not be used for the analysis.

For statistical reasons and due to computational limitations we preferred one-dimensional analysis of profiles to two-dimensional analysis of the surface. The two scanning directions of the tunneling microscope (the slow and the fast scanning directions) are not equivalent and they have different spectral components of noise. Although we have actually calculated $\mathscr{L}$ in both directions for some images, in most cases only the fast scan profiles were used.

For each image we analyzed the following functions, averaged over 400 profiles: the pair correlation function, $G(x)$, the power spectrum, $p(f)$, and the return probability histogram, $R(\Delta)$. The roughness exponent was calculated from the slopes of linear parts of the log–log plots of these functions according to eqs (12), (14), (16) and (19), respectively. We also constructed the correlation matrix M and the $\mathscr{L}$-function and analyzed them along the lines outlined in Section 4.

5.2. *Experimental Results*

We present in Figs 3–6 the averaged functions $G(x), p(f), P(f)$, and $R(\Delta)$ for graphite and for different regions of fractured tungsten surface. Each plot is marked with a value of H obtained from the slope of the linear part. Similar plots are given also for few noise images.

The intensity of the noise signal is few orders of magnitude lower than that of the recorded physical images, and therefore does not interfere with the spectral analysis. But the return probability histogram is not directly related to the amplitude of the signal. Therefore, from Fig. 6 alone we would not distinguish between the noise and the real signal.

Inspection of the power spectra of the graphite surface shown in Figs 4c and 5c leads to $H = 0.42 \pm 0.04$. The respective log–log plots do not display very long linear parts, especially for the higher resolution image (Fig. 2g). The same is true for the pair correlation function shown in Fig. 3b. The latter is characterized by $H = 0.34$ for the 700 nm scan and $H = 0.58$ for the 7000 nm scan. As we can see from the picture taken with the lowest resolution possible

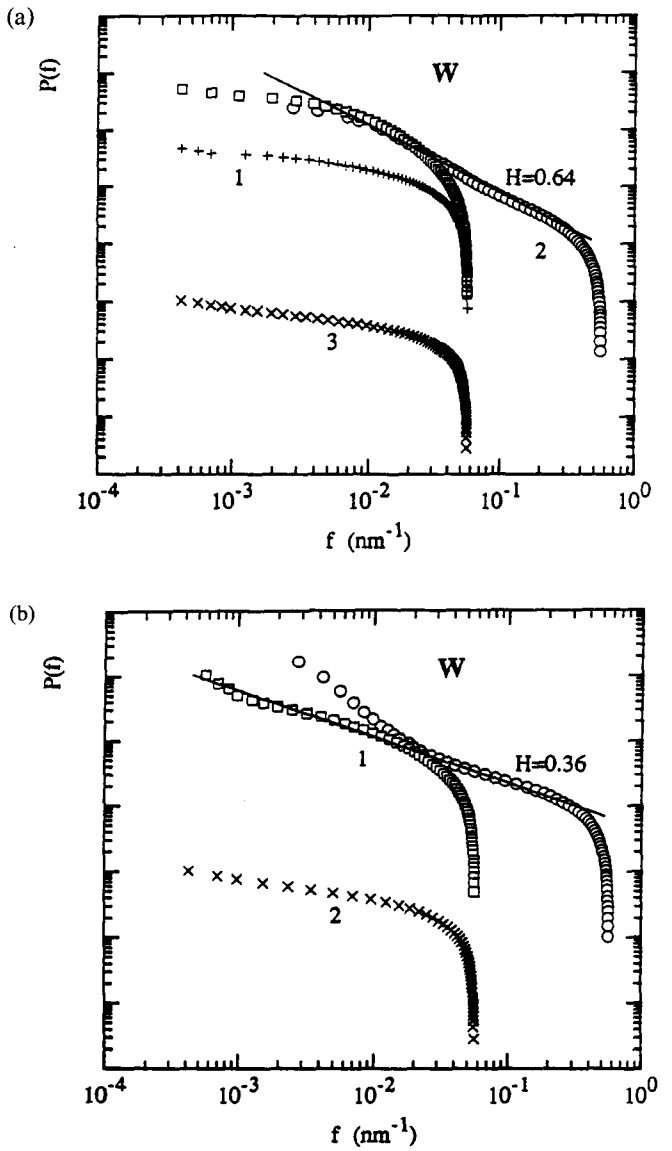

FIG. 5(a,b).

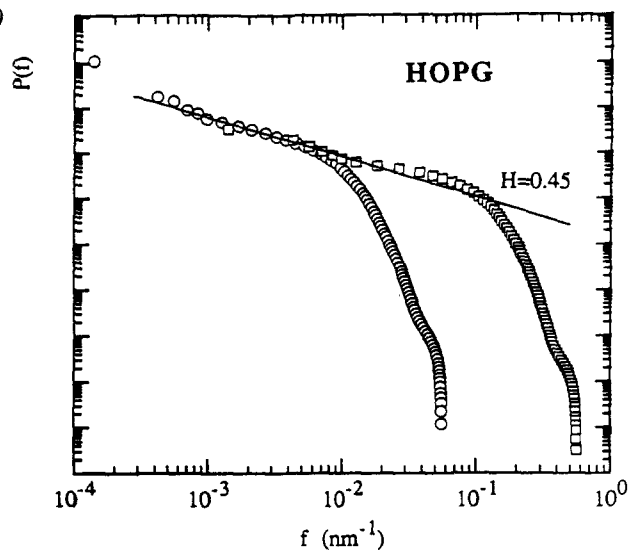

FIG. 5(c).

FIG. 5. The integrated power spectrum, $P(f)$. Notations as in Fig. 4.

for our STM, Fig. 2f, the graphite surface is irregular and contains a set of steps and ridges of seemingly arbitrary heights and orientations. At higher resolution there is usually no more than one pronounced feature, and other corrugations are on the atomic scale. These atomic-size corrugations are outside the fractal regime, and thus we can estimate the lower length-scale for scaling behaviour of the roughness of graphite surface to be at approximately 100 nm.

The first clear observation to be made for cleaved tungsten surface is that the least corrugated region, the mirror, cannot be described as a statistical fractal. All methods of analysis consistently suggest that for this part of the surface $H \approx 0$. We note that indeed the integrated power spectrum varies as $\log f$ rather than having a power law scaling.

A common feature of all other tungsten images is the presence of a structure of nearly parallel cleavage steps similar to those observed previously in STM study of brittle fracture surface of molybdenum.[65] These steps are the most pronounced microstructural element in our 700 nm scans. The difference between the regular stepped mist region and the crack branching part can be seen in the magnitude of corrugations between steps, see Figs 2c and 2e. The spectral analysis of these images reveals essentially linear scaling in logarithmic coordinates as shown in Figs 3–5. The roughness exponent is 0.66 ± 0.08 for the crack branching zone and 0.60 ± 0.10 for the regular stepped region.

In lower resolution tungsten images, Figs 2b and 2d, the steps appear as the secondary structural element imposed on a larger scale surface relief. This is manifested in Figs 3–5 for the mist region taken at two different length scales. In the crack branching zone the roughness of the surface is sufficient to blur out the steps as the main characteristic feature of the structure on 700 nm scale. This also corresponds to the short scale behaviour of $G(x)$ and of $p(f)$ for 7000 nm scan, shown in Figs 3a and 4a, that are characterized by $H = 0.60$, similar to the scaling of the higher resolution image. As the scanning length is increased to

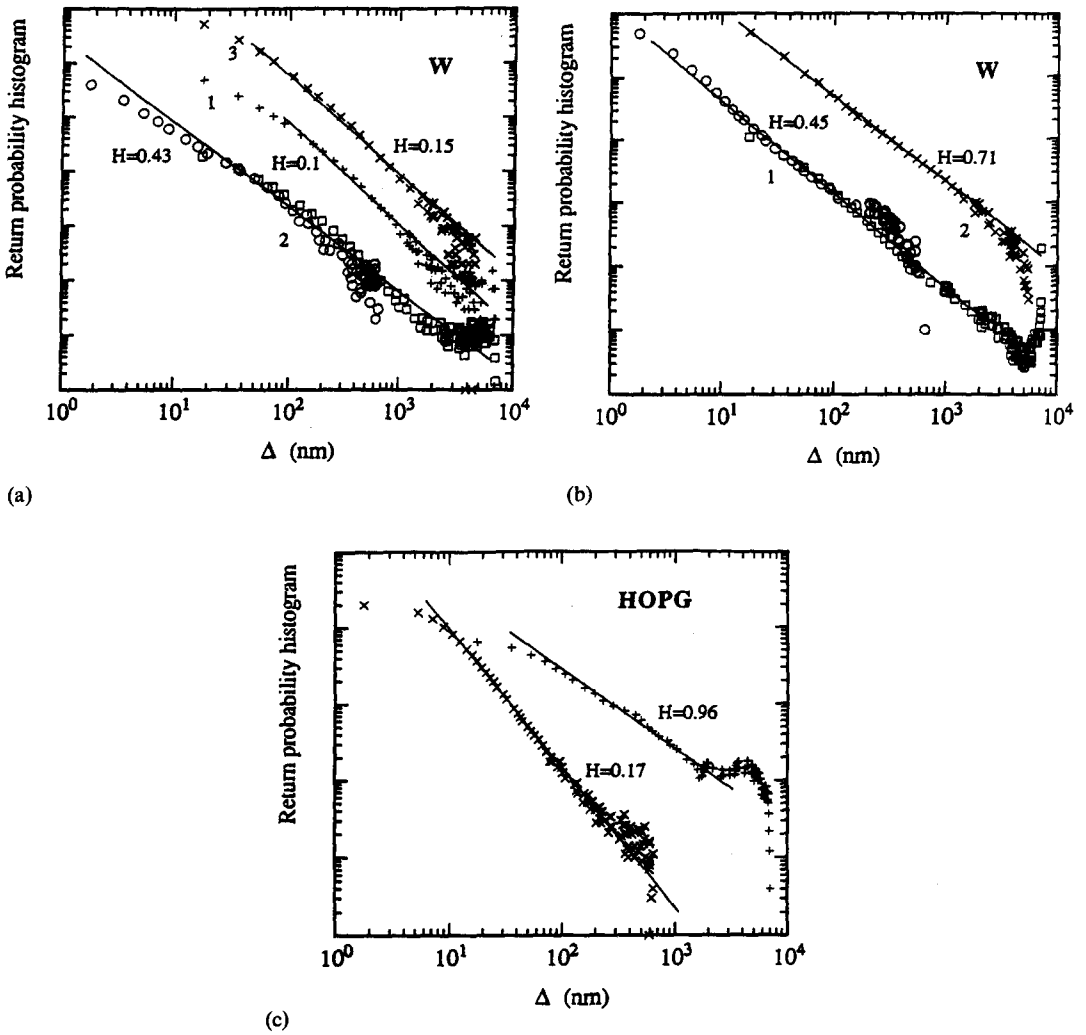

FIG. 6. The return probability histogram, R (Δ). Notations as in Fig. 4.

7000 nm, the regular stepped region exhibits nonlinear logarithmic plots, see Figs 3a and 4b. This change of behaviour could originate from the relatively short record length of 400 points, which may not be sufficient. Better statistics may enable to observe the change of the slope due to the change of the dominant element of structure as reported earlier by several authors.[4,14]

The pair correlation function, $G(x)$, can be calculated directly from eq. (8), with L being the scan length. We carried out such calculations in order to check the numerical stability of the conventional procedure based on the inverse Fourier transform of the power spectrum as given by eqs (13b) and (9). The only difference between the behaviour of the plots of $G(x)$ estimated by these two methods appears to be at separations between the behaviour of the scan length, which demonstrates their comparable performance for the analysis of the scaling behaviour.

To evaluate the length dependence of the profile width, $\omega(L_o)$, defined in eq. (10) we carried out another numerical real space integration. The scaling behaviour in eq. (18) is inferred from the scaling of the power spectrum at low spatial frequencies. Unfortunately, this part of $p(f)$ is the noisiest (see Fig. 4) and it is difficult to extract a reliable power law scaling from it. The question of how does the evaluation of H along the lines outlined in the previous paragraphs compare with the value that is derived from eq. (18) can be answered by comparing the plots of $\omega^2(L_o)$ and $G(x)$ in Fig. 7. These show that the resulting values of H are indeed similar. In the direct measurement using eq. (10) the averaging was carried out over all possible intervals of different length L_o and over all profiles contained in the STM image. For an ideally scaling surface both plots in Fig. 7 should display the same slope equal to $2H$. For tungsten surface we find that the two curves have indeed nearly constant and equal slopes and that they are similar over the entire range. This is a supporting argument of the scaling hypothesis, which also demonstrates the importance of cross-checking in roughness studies.

The return probability histogram shown in Fig. 6 appears to be less reliable for our purposes than the Fourier-analysis based methods. This is especially true for the graphite surface where the scale of the corrugation heights is much smaller than on the tungsten surface. The analysis of the return probability histogram for the low magnification images of tungsten gives $H = 0.42 \pm 0.05$ for the regular stepped region and 0.33 ± 0.05 for the rough crack branching zone. There is a discrepancy between the results obtained by this method and by the Fourier analysis. This discrepancy increases for higher magnification images when the absolute scale of the height of the surface features becomes smaller and the noise to signal ratio increases. The return probability histogram averaged over two different scan lengths yields for the regular stepped region $H = 0.45 \pm 0.06$, and $H = 0.43 \pm 0.05$ for the crack branching zone. The scaling parameter for the mirror region is correctly found to be close to zero. The roughness exponent for the graphite surface deducted from the return probability histogram (Fig. 6c) is difficult to relate to estimates from other methods. Most alarmingly, the return probability histogram gives a linear plot in logarithmic coordinates for the noise

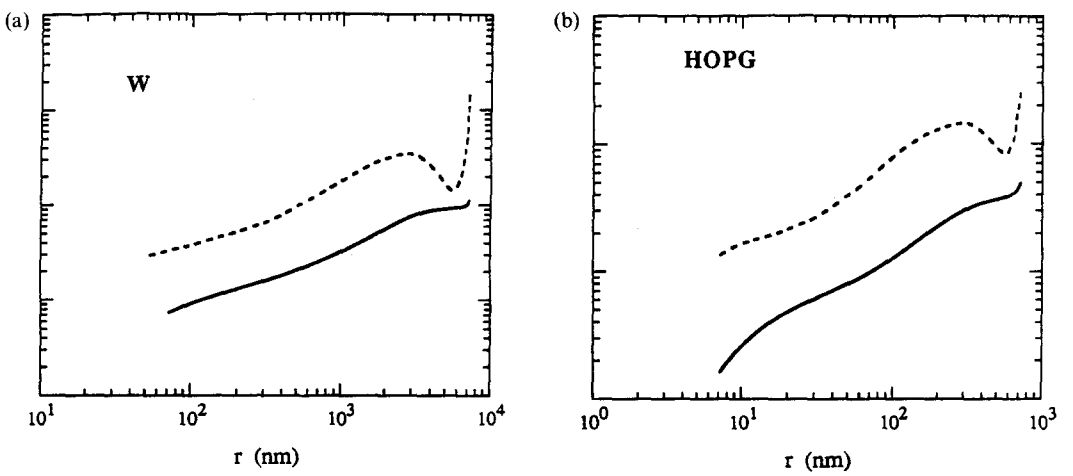

FIG. 7. The surface roughness squared, $\omega^2(L_0)$, solid line, as compared to the pair correlation function, $G(x)$, dashed line. Both functions evaluated using numerical integration according to eqs (8) and (10). (a) Regular stepped surface of tungsten; (b) Graphite.

image with $H = 0.71$! This is despite the fact that Fourier analysis does not show any scaling behaviour.

We now proceed to report a study of higher order correlations by analyzing the STM images with the aforementioned correlation matrix M and the $\mathscr{L}$-function. The plots of $\mathscr{L}$ for different parts of the tungsten surface are shown in Fig. 8. We observe that generally $\mathscr{L}$ starts from a large value and decays to unity over a scale of λ_s, which we have estimated for each particular plot. It is important to note that although in most cases $\lambda_s \geqslant 4$, we find that for the visually flat mirror region $\lambda_s \approx 2$. This serves as an encouraging check on the method since it indicates that correlations between scales decay faster in this region as one would expect. As a test system we analyzed a simulated flat surface with random noise (Fig. 8a). The plot of $\mathscr{L}$ shows that for the simple uncorrelated random noise the correlations between scales indeed die out much faster than in any of the real surfaces that we have studied. The rate of decay of $\mathscr{L}$ in the long range regime has the form

$$L = \alpha + A_p \exp(-p\,|\rho - \rho'|), \tag{35}$$

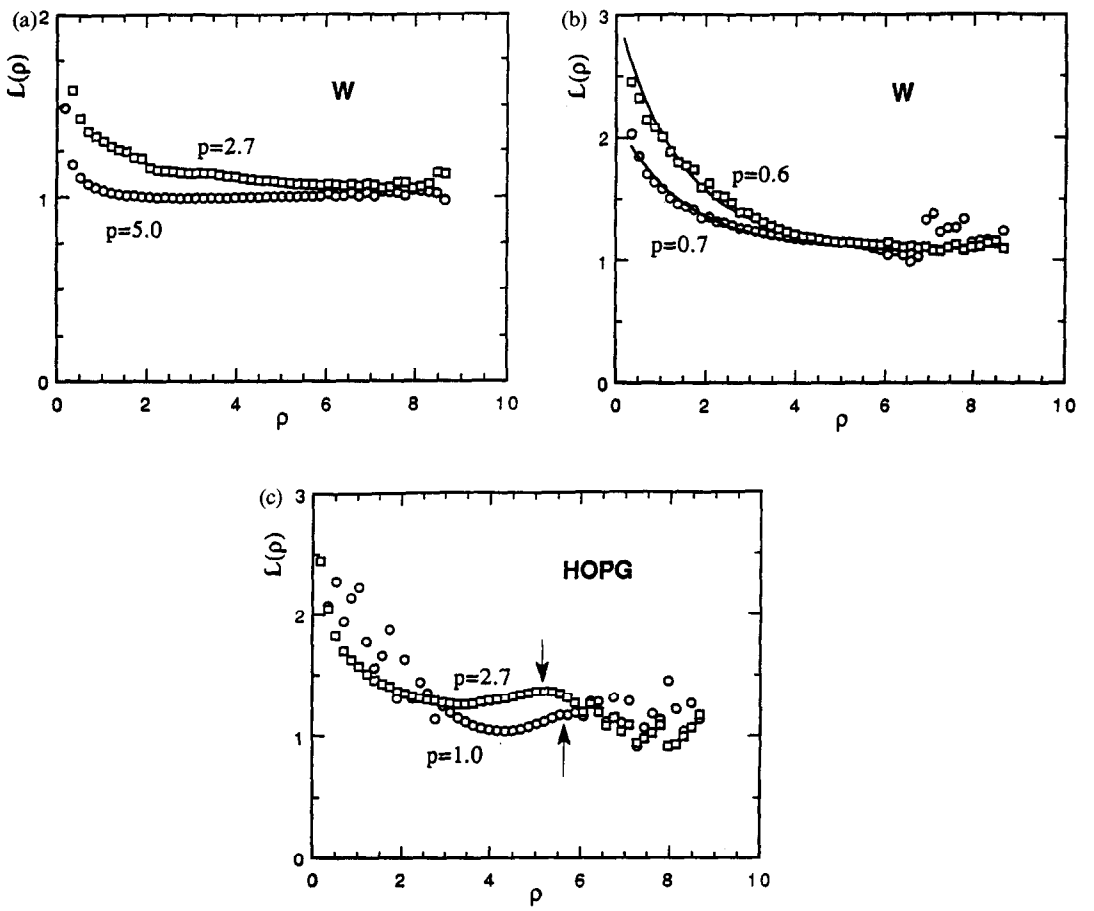

FIG. 8. The $\mathscr{L}$ (ρ) function: (a) mirror region on tungsten (squares) and flat simulated surface with random noise (circles); (b) tungsten; stepped mist (squares) and crack branching zone (circles). Solid lines show the results of least squares fit with eq. (35); (c) graphite; scan size of 7140 nm (circles) and 714 nm (squares).

where $\alpha = 1$ for asymptotically uncorrelated structures. At least in one case it has been shown that ρ exactly corresponds to the so-called higher order correction to scaling usually encountered in finite-size fractal systems.[10] It was further conjectured that ρ indeed relates to correction to scaling for general scale-invariant structures. Due to the relatively short scale of the data we did not attempt to fit the curve for p.

Analysis of the $\mathscr{L}$-function shows that size effects become pronounced at the short scales

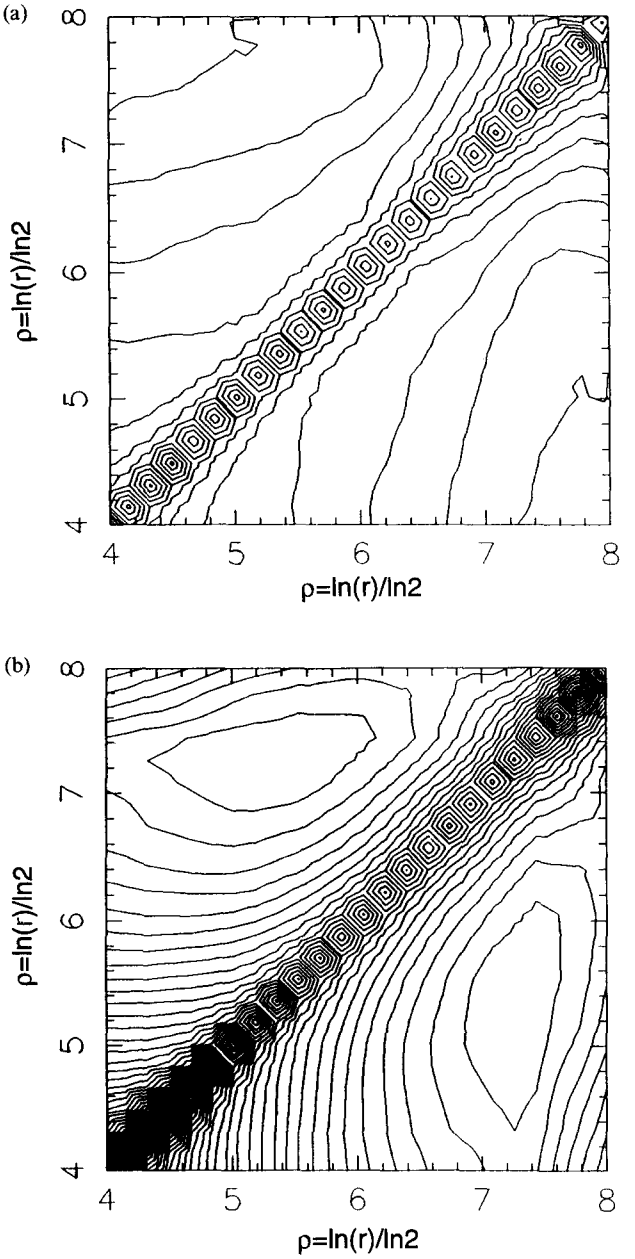

FIG. 9(a,b).

(c)

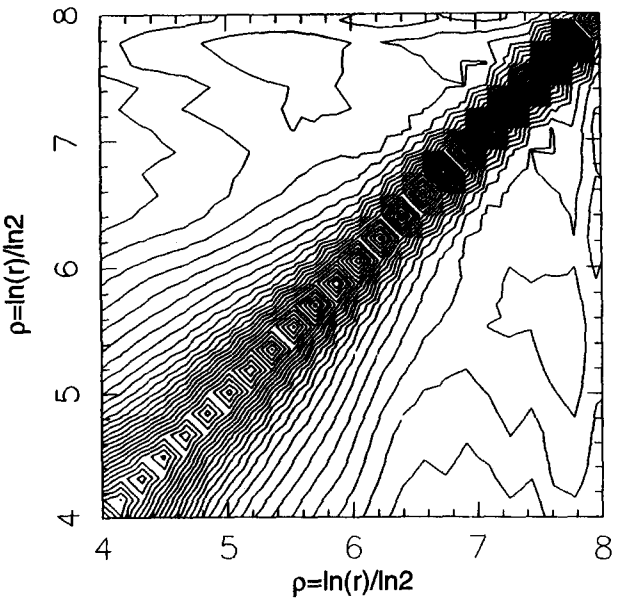

(d)

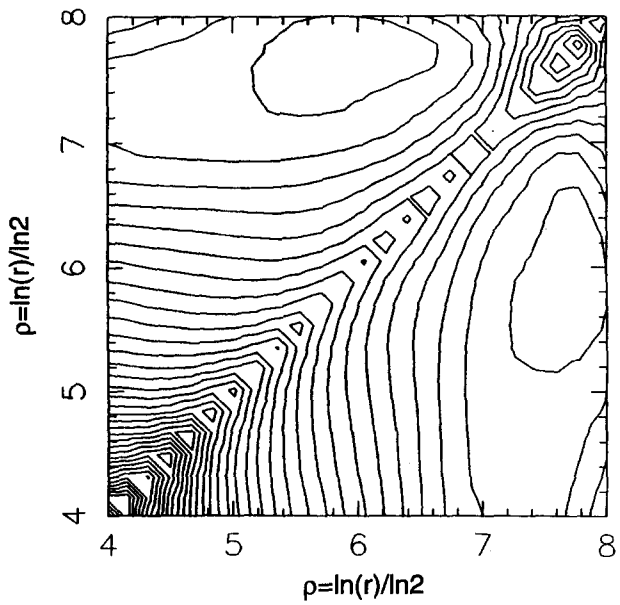

FIG. 9(c)–(d).

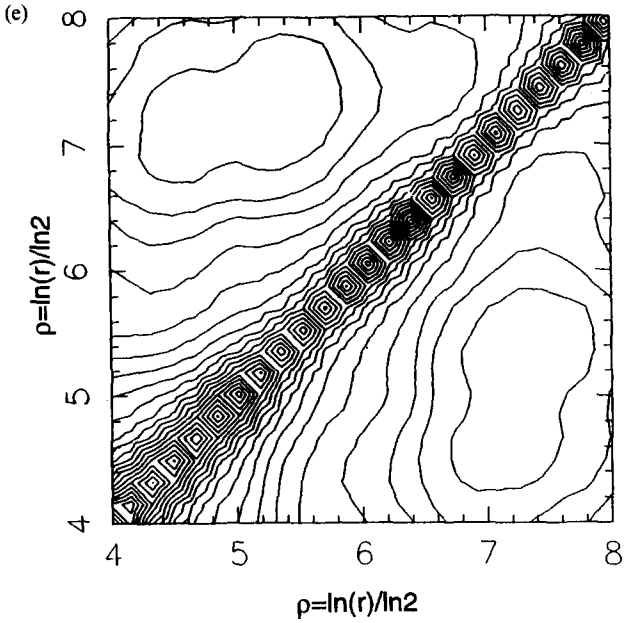

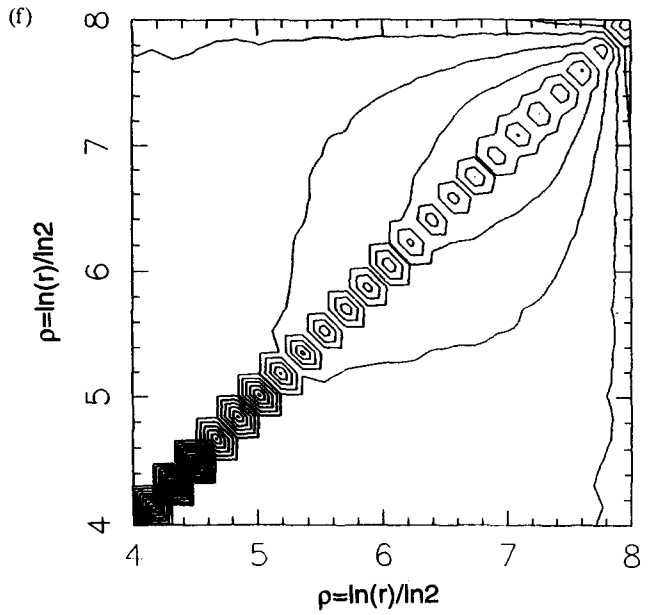

FIG. 9(e,f).

FIG. 9. Contour plots of the correlation matrix, $M(\rho, \rho')$: (a) tungsten mirror; (b) tungsten, stepped mist, scan length 7140 nm; (c) tungsten, crack branching zone, scan length 714 nm; (d) graphite, scan length 7140 nm; (e) graphite, scan length 714 nm; (f) simulated flat surface with random noise.

where the width of the shells becomes comparable to the grid size. We also note that the plots in Fig. 8 saturate to approximately unity ($\alpha = 1$) over a typical range of $|\rho - \rho'| \approx 4$–5. Graphite is the exception in two aspects: (i) The saturation range is shorter, between 2 and 3, indicating faster decay of hierarchical correlations; (ii) The plot of $\mathscr{L}$ has a small hump at $|\rho - \rho'| \approx 5.5$ (Fig. 8c). The latter can also be observed in the contour plot of the correlation matrix in Figs 9d and 9e. This value corresponds to $\log_2 5.5 \approx 45$, which indicates that there is a large contribution to the correlations from features occurring at this ratio of scales. This main characteristic feature in these systems consists of the irregularities that are visible in Fig. 2f, which are on scale of order of 2000 nm. The signal is therefore dominated by the ratio of this length-scale to finite-size characteristic features that appear at the small shell sizes, i.e. of order of ≈ 40 nm.

Inspecting the correlation matrix shown in Fig. 9, we observe that there is a significant difference between the morphologies of the mirror and the stepped regions of the tungsten surface. The only feature in the correlation matrix for the mirror is a steep ridge on the diagonal, see Fig. 9a. This effect is interpreted as indicating a very fast decay of the correlations. In contrast, the contour plots of M for different images of the stepped region (Figs 9b and 9c) reveal a much richer structure, indicating that the corrections decay much slower. Note though that the essential feature of these contours is that they are clearly parallel to the diagonal, pointing to the scale-invariant nature of the surface.

To summarize our results in this section, we carried out an extensive analysis on STM data in the nanometer scale, using many of the aforementioned different methods. These results show unambiguously that the mirror region of the tungsten fracture surface is microscopically flat and cannot be described as a fractal. We find that the regular stepped mist region is indeed self-affine with a roughness exponent $H = 0.46 \pm 0.10$, while for the rough track branching zone of tungsten surface $H = 0.61 \pm 0.10$. The scaling interval is, like in almost all other studies, not larger than two decades, which lends more weight to our analysis of third order correlations. The scale-invariant description is less satisfactory for the graphite surface. Although in this case the usual analysis of pair correlations indicates a possible self-affine surface with $H = 0.48 \pm 0.10$, the correlation matrix for this surface exhibits too complicated a structure to be consistent with a simple fractal.

In all cases we find that the values of H is substantially lower than the roughness exponent in the mesoscopic regime, which agrees with previous conclusions from STM studies.[44,47] This indeed suggests that the fracture processes in the two regimes are fundamentally different. Further theoretical investigation into this issue is required to explain exactly why nanometer-scale fracture are generally smoother than fractures on the mesoscopic scale.

6. Summary of Conclusions

We presented in this paper an extensive review of existing techniques for the analysis of fracture surfaces and of the results reported in the literature for a variety of materials. Our original intention was to include all the reliable data available so far, but new results in this field appear at such a rate that the data review section is doomed to become incomplete even before the publication. Nevertheless, we hope that our critical analysis of the existing status of the research will be useful for: (i) better understanding of the fundamental processes that lead to formation of fracture surfaces; (ii) determining the connection between the characteristic signatures of the fracture structures and the materials properties.

This review demonstrates quite clearly that there is no universal value of the roughness exponent that holds for all materials under arbitrary fracture conditions and on any length

scale. The first difficulty originates from the fact that the entire scale-invariant behaviour spans only two decades, which is the lowest possible range of scales that supports scaling. But the strongest evidence against universality comes from the large dispersion of the results for H in the mesoscopic regime that exist in the literature—between 0.6 and 1. Such a spread *in the exponent* represents a very broad distribution of the underlying experimental data and is difficult to reconcile with the hypothesis of universality.

This explains why there is still no agreement regarding the relation between the roughness exponent (or the fractal dimension of the fracture surface) and fracture toughness or any other single mechanical property. There is however a wide-spread consensus that is supported by most of the results that brittle fractures usually exhibit higher fractal dimensions for materials with higher toughness. In contrast, for ductile fractures, if there is some such correlation, it is very difficult to determine whether the roughness exponent increases or decreases with toughness. A good news, however, is that the scaling hypothesis has been firmly established by most studies and for many materials.

Fractal analysis of fracture structures is still a new and rapidly developing field that needs new ideas and new techniques. The above conclusions suggest that there is still much work to be done in this field for both physicists and material scientists. A challenge to the former community is to identify and then understand the principles that govern the mechanisms that lead to particular fracture characteristics. Specifically, this problem involves study of the short-time and long-time crack evolution within dynamical theory of fracture. The lack of fundamental understanding of this issue is sharpened by the wide scatter of results. One of the problems that needs to be studied is what causes the differences between the nano- and the micrometer scales. From a different angle, the main goal of materials scientists in this context is to find clues in the structure of fracture surfaces to the fundamental material properties. The conclusion of this review that fracture surfaces are *not universal* should come as good news to this community. Namely, universality would doom such a quest because its very existence would mean that there can be no correlations between material's properties and the scaling behaviour. A complication for the purposes of this community is the fact that the scaling regime is rather limited. This, combined with the wide dispersion of the values of H, suggests that scaling analysis alone is not sufficient neither to characterize fractures nor to correlate their structure with toughness or other mechanical properties.

To assist with this problem one possible addition to the tool kit of workers on this problem is a scheme for the study of higher-order correlations for obtaining information beyond that contained in the single parameter of the roughness exponent. This would complement the traditional scaling analysis and can be very useful in characterizing fractures of similar roughness exponent but different morphologies. To initiate steps in this direction we applied here a recently-introduced correlation scheme that probes three-point correlations between hierarchical scales. This analysis indeed shows that there are details that are essential to the structures, yet which are not accessible to the usual scaling analyses. This direction should assist in search for model materials by providing more detailed information on the signatures fracture surfaces. Another approach would be to attack the problem of the limited scaling regime. For example, one can eliminate the influence of grain boundaries by using single crystals, which may lead to an increase of the scaling window. Unfortunately, the price exacted by using these materials is that they are anisotropic, which complicates the analysis and the very fracture process. Yet another possibility in this direction is to further study fractures in glasses. It seems to us that attempts to analyze properties of multiphase materials (composites, dual-phase steels, alloys with precipitation hardening) are premature at this stage, when we cannot yet answer fundamental questions for simpler systems. From the

numerical point of view, an effort beyond simple modeling[7] is needed to understand the problem of fractal cracks at least in brittle materials.[32] Moreover, we suggest that more emphasis should be put on cross-checking of the numerical models with real fractures, and understanding the ranges of validity of such models.

ACKNOWLEDGEMENTS

We are pleased to acknowledge fruitful discussions of certain aspects of this paper with R. C. Ball, L. M. Brown, M. G. Walls and E. Bouchaud. We are grateful to all authors who kindly provided information on their research prior to publication of their results. Research of V.Y.M. was in part sponsored by the Division of Materials Sciences, U.S. Department of Energy, under contract DE-AC05-84OR21400 with Martin Marietta Energy Systems, Inc., by appointment to the Oak Ridge National Laboratory Postdoctoral Research Program administered by the Oak Ridge Institute for Science and Education. N.A.S. is grateful to Wolfson College, Cambridge, for Ribbands Studentship. R.B. acknowledges partial support from Los Alamos National Laboratory and grant DE-FG02-92ER14275.

REFERENCES

1. B. B. MANDELBROT, *The Fractal Geometry of Nature*. Freeman, San Fransisco (1982).
2. J. FEDER, *Fractals*. Plenum, New York (1988).
3. K. FALCONER, *Fractal Geometry*. J. Wiley, Chichester (1990).
4. B. B. MANDELBROT, D. E. PASSOJA and A. J. PAULLAY, *Nature* **308,** 721 (1984).
5. C. W. LUNG and Z. Q. MU, *Phys. Rev.* **B38,** 11781 (1988).
6. L. V. MEISEL, *J. Phys. D: Appl. Phys.* **24,** 942 (1991).
7. H. J. HERRMANN, *Fractals and Disordered Systems* (edited by A. BUNDE and S. HAVLIN). Springer, Berlin (1991).
8. K. J. MÅLØY, A. HANSEN, E. L. HINRICHSEN and S. ROUX, *Phys. Rev. Lett.* **68,** 213 (1991).
9. E. BOUCHAUD, G. LAPASSET and J. PLANÈS, *Europhys. Lett.* **13,** 73 (1990).
10. R. BLUMENFELD and R. C. BALL, *Phys. Rev.* **E38,** 11781 (1993).
11. R. BLUMENFELD and R. C. BALL, *Fractals*, in preparation (1994).
12. C. S. PANDE, L. R. RICHARDS and S. SMITH, *J. Mater. Sci. Lett.* **6,** 295 (1987).
13. E. BOUCHAUD, G. LAPASSET, J. PLANÈS and S. NAVEOS, *Phys. Rev.* **B48,** 2917 (1993).
14. R. H. DAUSKARDT, F. HAUBENSAK and R. O. RITCHIE, *Acta Metall. Mater.* **38,** 143 (1990).
15. E. E. UNDERWOOD and K. BANERJI, *Mater. Sci. Eng.* **80,** 1 (1986).
16. Q. Y. LONG, S. LI and C. W. LUNG, *J. Phys. D: Appl. Phys.* **24,** 602 (1991).
17. B. DUBUC, J. F. QUINION, C. ROQUES-CARMES, C. TRICOT and S. W. ZUCKER, *Phys. Rev.* **A39,** 1500 (1989).
18. S. MILLER and R. REIFENBERGER, *J. Vac. Sci. Technol.* **B10,** 1203 (1992).
19. L. E. RICHARDS and B. D. DEMPSEY, *Scr. Metall.* **22,** 687 (1988).
20. K. K. RAY and G. MANDAL, *Acta Metall. Mater.* **40,** 463 (1992).
21. Yu. A. KRUPIN and I. K. KISELEV, *Scr. Metall. Mater.* **24,** 2113 (1990).
22. Yu. A. KRUPIN and I. K. KISELEV, *Scr. Metall. Mater.* **25,** 655 (1991).
23. C. W. LUNG and S. Z. ZHANG, *Physica* **D38,** 241 (1989).
24. J. NOGUÉS, J. L. COSTA and K. V. RAO, *Physica* **A182,** 532 (1992).
25. Z. H. HUANG, J. F. TIAN and Z. G. WANG, *Scr. Metall. Mater.* **24,** 967 (1990).
26. Z. H. HUANG, J. F. TIAN and Z. G. WANG, *Mater. Sci. Eng.* **A118,** 19 (1989).
27. D. R. DENLEY, *Ultramicroscopy* **33,** 83 (1990).
28. J. J. FRIEL and C. S. PANDE, *J. Mater. Res.* **8,** 100 (1993).
29. J. K. KJENS, *Fractals and Disordered Systems* (edited by A. BUNDE and S. HAVLIN). Springer, Berlin (1991).
30. B. SAPOVAL, *Fractals and Disordered Systems* (edited by A. BUNDE and S. HAVLIN). Springer, Berlin (1991).
31. A. IMRE, T. PAYKOSSY and L. NYIKOS, *Acta Metall. Mater.* **40,** 1819 (1992).
32. R. C. BALL and R. BLUMENFELD, *Phys. Rev. Lett.* **65,** 1784 (1990).
33. R. V. GOLDSTEIN and A. B. MOSOLOV, *Doklady AN SSSR* **319,** 840 (1991) (in Russian); V. V. SILBERSCHMIDT, *Europhys. Lett.* **23,** 593 (1993); A B. MOSOLOV, *Europhys. Lett.* **24,** 673 (1993).
34. D. STAUFFER and A. AHARONY, *Introduction to Percolation Theory*. Taylor & Francis, London, (1992).
35. T. KLEISER and M. BOCEK, *Z. Metallkde.* **77,** 582 (1986).
36. B. SPRUSIL and F. HNILICA, *Czech J. Phys.* **B35,** 897 (1985).
37. K. ISHIKAWA, T. OGATA and K. NAGAI, *J. Mater. Sci. Lett.* **8,** 1326 (1989).
38. B. SPRUSIL, H. U. FRITSCH and B. L. MORDIKE, *Z. Metallkde.* **79,** 50 (1988).

39. A. HANSEN, E. L. HINRICHSEN and S. ROUX, *Phys. Rev. Lett.* **66,** 2476 (1991).
40. S. ROUX and D. FRANÇOIS, *Scr. Metall. Mater.* **25,** 1087 (1991).
41. M. KARDAR and Y. C. ZHANG, *Europhys. Lett.* **8,** 233 (1989).
42. J. J. MECHOLSKY, JR. and S. W. FREIMAN, *J. Amer. Ceram. Soc.* **74,** 3136 (1991).
43. Y. L. TSAI and J. J. MECHOLSKY, JR, *J. Mater. Res.* **6,** 1248 (1991).
44. S. C. LANGFORD, MA ZHENYI, L. C. JENSEN and J. T. DICKINSON, *J. Vac. Sci. Technol.* **A8,** 3470 (1990).
45. J. J. MECHOLSKY, D. E. PASSOJA and K. S. FEIBERG-RINGEL, *J. Am. Ceram. Soc.* **72,** 60 (1989).
46. J. J. MECHOLSKY, JR and J. R. PLAIA, *J. Non-Cryst. Solids* **146,** 249 (1992).
47. M. W. MITCHELL and D. A. BONNELL, *J. Mater. Res.* **5,** 2244 (1990).
48. J. J. MECHOLSKY and T. J. MACKIN, *J. Mater. Sci. Lett.* **7,** 1145 (1988).
49. G. R. BARAN, C. ROQUES-CARMES, D. WAHBI and M. DEGRANGE, *J. Am. Ceram. Soc.* **75,** 2687 (1992).
50. G. M. LIN and J. K. L. LAI, *J. Mater. Sci. Lett.* **12,** 470 (1993).
51. MA ZHENYI, S. C. LANGFORD, J. T. DICKINSON, M. H. ENGELHARD and D. R. BAER, *J. Mater. Res.* **6,** 183 (1991).
52. A. M. BRANDT and G. PROKOPSKI, *J. Mater. Sci.* **28,** 4762 (1993).
53. V. E. SAOUMA, C. C. BARTON, and N. A. GAMALELDIN, *Eng. Fract. Mech.* **35,** 47 (1990).
54. S. KUMAR, G. BODVARSSON and J. BOERNGE, *High Level Radioactive Waste Management*, Vol. 2, 279 (1991).
55. J. KERTÉSZ, *Physica* **A191,** 208 (1992).
56. V. YU. MILMAN, *Mechanics of Creep of Brittle Materials* (edited by A. C. F. COCKS and A. R. S. PONTER) p. 124. Elsevier, Barking (1991).
57. V. YU. MILMAN, R. BLUMENFELD, N. A. STELMASHENKO and R. C. BALL, *Phys. Rev. Lett.* **71,** 204 (1993).
58. Z. Q. MU and C. W. LUNG, *Theor. Appl. Fract. Mech.* **17,** 157 (1992).
59. Z. Q. MU, C. W. LUNG, Y. KANG and Q. Y. LONG, *Phys. Rev.* **B48,** 7679 (1993).
60. I. PRZERADA and A. BOCHENEK, *Acta Sterologica* **11,** Suppl. 1, Vol. 2, 343 (1992).
61. V. K. HORVÁTH and H. J. HERRMANN, *Chaos Solitons Fractals* **1,** 395 (1991).
62. Q. Y. LONG, JUN CHEN, JIZHI CHEN, Z. Q. MU, and C. W. LUNG, *Scr. Metall. Mater.* **27,** 1319 (1992).
63. Y. FAHMY, J. C. RUSS, and C. C. KOCH, *J. Mater. Res.* **6,** 1856 (1991).
64. H. YAO, T. JIFENG, and W. ZHONGGUANG, *Mater. Sci. Eng.* **A148,** 45 (1991).
65. H. SUMIYOSHI, S. MATSUOKA, K. ISHIKAWA and M. NIHEI, *JSME Int. J. Series I* **35,** 449 (1992).
66. S. MATSUOKA, H. SUMIYOSHI and K. ISHIKAWA, *Trans. Jpn. Soc. Mech. Eng.* (in Japanese) **56,** 2091 (1990).
67. M. TANAKA, *J. Mater. Sci.* **27,** 4717 (1992); *ibid.* **28,** 5753 (1993).
68. Z. G. WANG, D. L. CHEN, X. X. JIANG, S. H. AI and C. H. SHIH, *Scr. Metall.* **22,** 827 (1988).
69. P. MCANULTY, L. V. MEISEL and P. J. COTE, *Phys. Rev.* **A46,** 3523 (1992).
70. H. SU, Y. ZHANG and Z. YAN, *Scr. Metall. Mater.* **25,** 651 (1991).
71. T. SHIBAYANAGI, O. YAMAMOTO and S. HORI, *Mater. Trans. JIM* **31,** 225 (1990).
72. K. ISHIKAWA, *J. Mater. Sci. Lett.* **9,** 400 (1990).
73. X. G. JIANG, W. Y. CHU and C. M. HSIAO, *Acta Metall. Mater.* **42,** 105 (1994).
74. A. W. THOMPSON and M. F. ASHBY, *Scr. Metall.* **18,** 127 (1984).
75. D. L. DAVIDSON, *J. Mater. Sci.* **24,** 681 (1989).
76. C. S. PANDE, L. E. RICHARDS, N. LOUAT, B. D. DEMPSEY and A. J. SCHWOEBLE, *Acta Metall.* **35,** 1633 (1987).
77. E. HORNBOGEN, *Int. Mater. Rev.* **34,** 277 (1989).
78. X. G. JIANG, J. Z. CUI and L. X. MA, *J. Mater. Sci. Lett.* **12,** 1616 (1993).
79. G. BINNIG and H. ROHRER, *Helv. Phys. Acta* **55,** 726 (1982).
80. M. G. WALLS, *Ann. Chim. Fr.* **17,** 191 (1992).
81. R. HIESGEN and D. MEISSNER, *Ultramicroscopy* **42–44,** 1403 (1992).
82. M. MÜLLER, H. VEHOFF and P. NEUMANN, *Ultramicroscopy* **42–44,** 1412 (1992).
83. Nanoscope II, Digital Instruments Inc., Santa Barbara, CA 93110, USA.

APPENDIX

We consider here the effect of the subtraction of the linear background on calculated width, ω, of the height profile. Our aim is to show that the least squares fitted slope of the background minimizes ω.

Consider a physical profile $h(x)$ and a corrected profile

$$g(x) = h(x) - ax - b. \tag{A1}$$

The width of $h(x)$, ω_0, given by eq. (10):

$$\omega_0^2 = \langle (h - \langle h \rangle)^2 \rangle = \langle h^2 \rangle - \langle h \rangle^2. \tag{A2}$$

Using (A1) and (A2) we can relate the widths of g and h by

$$\omega^2 = \omega_0^2 + a(L_0 \langle h \rangle - 2\langle xh(x) \rangle) + a^2 L_0^2/12. \tag{A3}$$

The width depends only on the slope a and not on the constant shift b. The difference between the widths is quadratic in a and is minimized for $a = a_{\min}$:

$$a_{\min} = \frac{6}{L_0^2}(2\langle xh(x)\rangle - L_0\langle h\rangle). \tag{A4}$$

The least square fitting procedure is in this case equivalent to minimizing $\langle g^2\rangle$:

$$\langle g^2\rangle = \langle h^2\rangle - 2a\langle xh(x)\rangle - 2b\langle h\rangle + \tfrac{1}{3}a^2L_0^2 + abL_0. \tag{A5}$$

The solution is found in the usual way by differentiating (A5) with respect to a and b which gives:

$$a_{\text{lsf}} = \frac{6}{L_0^2}(2\langle xh(x)\rangle - L_0\langle h\rangle), \tag{A6a}$$

$$b_{\text{lsf}} = 4\langle h\rangle - \frac{6}{L_0}\langle xh(x)\rangle. \tag{A6b}$$

Relation (A6a) is identical to (A4), confirming that the same slope is obtained by either minimizing the width of the resulting profile or by carrying out conventional least squares fit to the tilted profile.